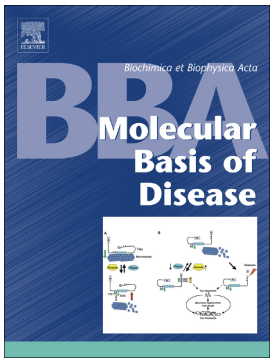

Myelin-associated glycoprotein activation triggers glutamate uptake by oligodendrocytes in vitro and contributes to ameliorate glutamate-mediated toxicity in vivo

Ana L. Vivinetto, Clara Castañares, Constanza Garcia-Keller, Ana Lis Moyano, Cristian Falcon, Anabela Palandri, Victoria Rozés-Salvador, Juan I. Rojas, Liliana Patrucco, Clara Monferran, Liliana Cancela, Edgardo Cristiano, Ronald L. Schnaar, Pablo H.H. Lopez

PII: S0925-4439(21)00257-X

DOI: https://doi.org/10.1016/j.bbadis.2021.166324

Reference: BBADIS 166324

To appear in: *BBA - Molecular Basis of Disease*

Received date: 10 September 2021

Accepted date: 8 December 2021

Please cite this article as: A.L. Vivinetto, C. Castañares, C. Garcia-Keller, et al., Myelin-associated glycoprotein activation triggers glutamate uptake by oligodendrocytes in vitro and contributes to ameliorate glutamate-mediated toxicity in vivo, *BBA - Molecular Basis of Disease* (2021), https://doi.org/10.1016/j.bbadis.2021.166324

Title: Myelin-associated glycoprotein activation triggers glutamate uptake by oligodendrocytes in vitro and contributes to amielorate glutamate-mediated toxicity in vivo.

Running title: MAG activation induces glutamate uptake

Ana L. Vivinetto[1], Clara Castañares[1], Constanza Garcia-Keller[2], Ana Lis Moyano[4], Cristian Falcon[3], Anabela Palandri[1], Victoria Rozés-Salvador[1], Juan I Rojas[5], Liliana Patrucco[5], Clara Monferran[3], Liliana Cancela[2], Edgardo Cristiano[5], Ronald. L. Schnaar[6,7] and Pablo H.H. Lopez[1,3,8, 9].

[1]*Laboratorio de Neurobiología, Instituto de Investigación Médica Mercedes y Martin Ferreyra, INIMEC-CONICET-Universidad Nacional de Córdoba, Argentina.*

[2]*Departamento de Farmacología-IFEC-CONICET and [3]Departamento de Química Biológica Dr. Ranwell Caputto-CIQUIBIC-CONICET; Facultad de Cs Químicas; Universidad Nacional de Córdoba, Argentina.*

[4]*Instituto Universitario de Ciencias Biomédicas de Córdoba-IUCBC, Córdoba, Argentina*

[5]*Centro de Esclerosis Múltiple de Buenos Aires-CEMBA, Hospital Italiano de Buenos Aires, Argentina.*

[6]*Departments of Pharmacology and [7]Neuroscience, Johns Hopkins University School of Medicine, Baltimore, MD, USA.*

[8]*Facultad de Psicología, Universidad Nacional de Córdoba, Argentina.*

[9]*To whom correspondence should be addressed: e-mail: pablo.lopez@unc.edu.ar*

Manuscript Correspondence to:

Dr. Pablo H. H. Lopez

Departamento de Química Biológica "Dr Ranwell Caputto", Facultad de Ciencias Químicas, CIQUIBIC-CONICET-Universidad Nacional de Córdoba.

Av. Haya de la Torre s/n, Pabellón Argentina, Ciudad universitaria, Córdoba, X5000HUA, Provincia de Córdoba, Argentina. +54-351-5353855 (voice)

pablo.lopez@unc.edu.ar

Abbreviations: Oligodendrocytes, OLs; Myelin-associated glycoprotein, MAG; multiple

sclerosis, MS; glutamate, Glu; reduced glutathione, GSH; excitatory aminoacid transporters, EAATs; aminoadipic acid, AAA; L-trans-pyrrolidine-2,4-dicarboxylate, PDC; Föster resonance energy transfer, FRET; factor nuclear erythroid-related factor 2, Nrf2; phosphatidylinositol 4,5-bisphosphate, PIP2; diacylglycerol, DAG; phospholipase C gamma, PLCγ; antioxidant response element, ARE, regulatory light chain of system xc transporter, xCT; glutathione reductase (GSR), catalytic and the regulatory subunits of the glutamate-cysteine ligase, Gclc and Gclm, respectively; ribosomal protein l13A, rpl13, Experimental Autoimmune Encephalomyelitis, EAE, normal horse serum, NHS; David Garcia-Callejas, DGC.

Keywords: Oligodendrocyte, glutamate, neuroprotection, neurodegeneration, excitotoxicity, myelin, Multiple Sclerosis, experimental autoimmune encephalomyelitis, Myelin-associated glycoprotein, stroke.

Acknowledgments

This work was supported by grants FONCyT PICT-2013-2416, Secyt-UNC category A to P.H.H.L, Merck KGaA award to P.H.H.L and E.C and NIH grant MH107965 to R.L.S. A.L.V., A.P, C.G.K. C.C, V.R.S and C.F. were supported by fellowships from CONICET. A.L.M, C.M., L.C. and P.H.H.L. are researchers from CONICET. The authors thank Dr. S. Barnett-U. Glasgow for critical reading of the manuscript.

Conflict of interest

This research was supported by a grant (to PHHL and EC) from Merck KGaA, Darmstadt, Germany.

Highlights

- MAG activation in Oligodendrocytes induces extracellular glutamate uptake.
- MAG activation in Oligodendrocytes results in a PLC/PKC-mediated activation of Nfr2 leading to an antioxidant response.
- MAG activation results in neuroprotection against glutamate-mediated toxicity in vivo.

Abstract

BACKGROUND: Myelin-associated glycoprotein (MAG) is a key molecule involved in the nurturing effect of myelin on ensheathed axons. MAG also inhibits axon outgrowth after injury. In preclinical stroke models, administration of a function-blocking anti-MAG monoclonal antibody (mAb) aimed to improve axon regeneration demonstrated reduced lesion volumes and a rapid clinical improvement, suggesting a mechanism of immediate neuroprotection rather than enhanced axon regeneration. In addition, it has been reported that antibody-mediated crosslinking of MAG can protect oligodendrocytes (OLs) against glutamate (Glu) overload by unknown mechanisms. PURPOSE: To unravel the molecular mechanisms underlying the protective effect of anti-MAG therapy with a focus on neuroprotection against Glu toxicity. RESULTS: MAG activation (via antibody crosslinking) triggered the clearance of extracellular Glu by its uptake into OLs via high affinity excitatory amino acid transporters. This resulted not only in protection of OLs but also nearby neurons. MAG activation led to a PKC-dependent activation of factor Nrf2 (nuclear-erythroid related factor-2) leading to antioxidant responses including increased mRNA expression of metabolic enzymes from the glutathione biosynthetic pathway and the regulatory chain of cystine/Glu antiporter system xc^- increasing reduced glutathione (GSH), the main antioxidant in cells. The efficacy of early anti-MAG mAb administration was demonstrated in a preclinical model of excitotoxicity induced by intrastriatal Glu administration and extended to a model of Experimental Autoimmune Encephalitis showing axonal damage secondary to demyelination. CONCLUSIONS: MAG activation triggers Glu uptake into OLs under conditions of Glu overload and induces a robust protective antioxidant response.

Introduction

Identifying novel strategies to promote glutamate (Glu) clearance represents an important therapeutic approach to induce neuroprotection after injury. Glu overload and oxidative stress are key processes common to many neurodegenerative diseases including stroke and multiple sclerosis (MS) (Piani *et al.*, 1991; Stover *et al.*, 1997; Pitt *et al.*, 2000; Offen *et al.*, 2004; Srinivasan *et al.*, 2005; Pampliega *et al.*, 2011; Kostic *et al.*, 2013; Hohlfeld and Kerschensteiner, 2016; Macrez *et al.*, 2016; Morales-Pantoja *et al.*, 2016). High levels of extracellular Glu results in excessive stimulation of Glu receptors and subsequent excitotoxicity. Additionally, high Glu causes

receptor-independent toxicity via blockage of cystine uptake by the cystine/Glu antiporter system xc-, a critical step towards the production of reduced glutathione (GSH), the main antioxidant element in cells (Oka *et al.*, 1993; Takahashi *et al.*, 2003). The homeostasis of Glu is maintained via fast uptake by high affinity sodium-dependent excitatory amino acid transporters (EAATs) expressed by glial cells that remove and detoxify Glu from extracellular space (Nedergaard *et al.*, 2002). Astrocytes are key regulators of this process, but oligodendrocytes (OLs) also express Glu transporters and are thought to be the predominant glutamate metabolizing cells in human brain white matter (Pitt *et al.*, 2003; Werner *et al.*, 2001). Targeting a single glycoprotein expressed by myelinating cells with a critical role in bidirectional communication between myelin and axons (Quarles, 2007), Myelin-associated glycoprotein (MAG), exerts neuroprotection in animal models. Preclinical studies using a well characterized anti-MAG mAb (capable to block the inhibitory effect of MAG on axon regeneration) demonstrated clinical improvement in experimental stroke models (Irving *et al.*, 2005; Thompson *et al.*, 2006). The relatively rapid recovery observed in these experimental models suggest a neuroprotective effect instead of promoting a regenerative process (Barbay *et al.*, 2015; McKerracher and Rosen, 2015). Moreover antibody-mediated crosslinking of MAG in OLs leads to its activation and further protects them from death caused by extracellular Glu overload (Marta *et al.*, 2004; Irving *et al.*, 2005). Recently, the crystal structure of MAG was solved and the structural analysis identified key aminoacids or intracellular domains determining its homodimerization, which confirmed its potential impact on its bidirectional activity (Pronker *et al.*, 2016, Mylvaganam *et al.*, 2018). While there is, therefore, considerable evidence to support the notion that targeting OLs via MAG exerts early neuroprotection, the current underlying molecular mechanisms have yet to be fully established. In addition, clinical trials using a humanized version of this mAb failed to demonstrate clinical benefits in stroke patients (Cramer *et al.*, 2013, 2017), and the explanation of the efficacy differences between human and preclinical models remains to be unveiled. Answering these questions will provide knowledge to better understand the potential role of OLs in neuroprotection in order to develop novel therapeutic strategies. We hypothesize that the acute protection associated to anti-MAG therapy is related to the triggering of signaling cascades resulting in extracellular Glu clearance by OLs. We addressed these questions by investigating the mechanisms and molecular pathways leading to neuroprotection by OLs using *in vitro* and *in vivo* models of Glu toxicity. We unmask a novel capacity of OLs to uptake Glu in conditions of Glu overload and to activate a robust antioxidant response with the potential to be exploited therapeutically. Also, our data demonstrate that activation of MAG not only protects OLs but blocks the detrimental consequences of Glu overload on other resident cells of the CNS, leading to neuroprotection.

Results

Antibody-mediated activation of MAG increases GSH content in OLs and prevent Glu-mediated mitochondrial oxidative stress.

Crosslinking MAG using a well characterized anti-MAG mAb prevents Glu-mediated toxicity in OLs (Irving *et al.,* 2005). Glu-mediated toxicity in these cells is mostly exerted via oxidative stress (Oka *et al.,* 1993; Rosin *et al.*, 2004; Irving *et al.*, 2005); therefore, we first studied whether MAG activation in OLs could affect the concentration of GSH, the main cellular anti-oxidant element. Primary OL cultures were analyzed for their intracellular level of GSH by confocal microscopy using the fluorescent dye mBCl. Treatment of OL cultures for 24 h with 2 mM Glu significantly reduces GSH content while treatment with 2 µg/ml anti-MAG mAb induces ≈40% increase in GSH concentration ($F=17.74$ $p=0.0001$). No changes in GSH were observed in cultures treated with a similar dose of control mAb. Combined treatment with Glu and anti-MAG mAb resulted in a compensatory effect preventing Glu mediated-GSH depletion (**Figure 1a-b**). A time-course study indicated a robust increase in GSH within 10 h of treatment of OLs with anti-MAG mAb (≈80% of GSH levels determined at 24 h. under similar conditions) ($F=6.71$, $p=0.005$) (**Figure 1c**). Direct evidence of an antioxidant response triggered by MAG activation in mature OL cultures was obtained by transfection with a cDNA plasmid containing the sequence for mitoHyper, a selective H_2O_2 biosensor. Antibody–mediated activation of MAG in OL cultures for 24 h resulted in a significant reduction of mitochondrial H_2O_2 compared to control mAb-treated cultures ($T=-2.53$ $p=0.021$) (**Figure 1d-e**). Further studies in OL cultures using tetramethylrhodamine (TMRE), a live mitochondrial potential dye; showed that exposure to Glu resulted in increased fluorescence intensity (increased mitochondrial potential) suggesting early stages of cell death (Kumari *et al.,* 2012), while anti-MAG treatment prior to Glu exposure prevented mitochondrial potential hyperpolarization, with cultures depicting fluorescence intensities even below IgG-treated controls ($H=58.52$;*$p\leq0.05$) (**Figure 1f-g**).

Antibody-mediated activation of MAG promotes extracellular Glu uptake in OLs.

Since GSH is a tripeptide synthesized by conjugation of the amino acids Glu, cysteine and glycine, we next analyzed whether the protective effect of MAG relies on Glu uptake. The

antibody-mediated increase in GSH was prevented by pretreatment of OL cultures for 24 h with pharmacological inhibitors of cystine/Glu antiporter System xc^- (0.6 mM aminoadipic acid; AAA) ($F=28.73$ $p<0.0001$) and excitatory amino acid transporters (EAATs, 300 μM of L-trans-pyrrolidine-2,4-dicarboxylate; PDC) ($F=2.91$ $p=0.035$), which function in a concerted manner to maintain Glu homeostasis (Lewerenz *et al.*, 2006) (**Figure 2a**)**.** We then studied Glu flux across the OLs plasma membrane using a library of FRET-based Glu biosensors. OL cultures were transfected with pDisplay FLIPE 1m, a Glu biosensor with expression restricted to plasma membrane allowing extracellular Glu analysis. Then OLs were exposed for 24 h to anti-MAG mAb and further challenged for 1 h with 2 mM Glu. We observed that anti-MAG treatment resulted in a reduction of extracellular Glu ($F= 4.82$, $p=0.003$), suggesting its active uptake by OLs (**Figure 2b-c**). Cold colors indicated low FRET activity (high extracellular Glu) and warm colors represent high FRET activity (low extracellular Glu). This Glu flux was also confirmed by using FLIPE 10u, a Glu biosensor with expression restricted to the cytoplasm. OL cultures transfected with FLIPE 10u, treated with anti-MAG mAb for 24 h and further challenged with 2 mM Glu for 30 min displayed increased intracellular Glu when compared to control mAb-treated OLs ($F=17.72$, $p\leq0.0001$). Combined treatment of OLs with 300 μM PDC 1 h before anti-MAG treatment abolished Glu uptake (**Figure 2d-e**) *(*$F=3.55$, $p=0.016$*).* This effect was statistically significant when analyzing FRET activity either in OLs soma ($H= 8.11$ $p=0.043$; data not shown) or processes ($F=17.72$, $p<0.0001$). Active uptake of Glu was corroborated by using enzyme–based quantification of extracellular Glu by fluorimetry. While no change in extracellular Glu was observed at 1 h after anti-MAG treatment, a robust Glu uptake in OL cultures was observed at 24 h of anti-MAG treatment, which exhibit similar extracellular Glu values to IgG treated control cultures (*, $p\leq0.0001$; #, $p\leq0.05$). (**Figure 2f-g**). The discrepancy between the time-course of FRET-based and enzyme-based measurements most probably reflects net changes in the concentration of the membrane environment surrounding the biosensor (early) versus bulk (late) Glu concentrations at 1 and 24 h, respectively.

MAG activation results in a PKC-dependent phosphorylation/translocation of the transcription factor nuclear erythroid-related factor 2 (Nrf2) and further activation of antioxidant response elements (ARE) signaling pathway.

In another set of experiments, we studied the mechanisms underlying the protective effect of MAG against Glu overload. OL cultures were treated with anti-MAG antibody and expression of the active form of a key regulator of cellular anti-oxidant response signaling pathways,

transcription factor nuclear erythroid-related factor 2 (Nrf2) phosphorylated at serine 40 (Nrf2-serine-40), was analyzed by confocal microscopy. We observed an increased nuclear translocation/activation of Nrf2-serine-40 10 h after MAG activation compared to control-treated cultures ($F=5.75$, $p<0.002$) (**Figure 3a-b**). This result was confirmed by Western blot in cell homogenates from OL cultures. Anti-MAG treatment significantly increased the amount of Nrf2-serine-40 compared to control mAb-treated cultures (ratios of 5.1 to 6.9 for high and low MW Nrf2-serine-40 when normalized against control IgG, respectively) (**Figure 3c**). Nrf2 phosphorylation/activation at serine 40 is mediated by protein kinase C (PKC) activity (Huang *et al.*, 2002; Bloom and Jaiswal, 2003, Lau et al, 2013). Similarly. the cytoplasmic region of MAG predominantly expressed in the CNS binds to and activates the PKC activator phospholipase Cγ (PLCγ) in vitro (Kirchhoff *et al.*, 1993; Jaramillo *et al.*, 1994). Therefore, we hypothesized that MAG could induce the activation of the ARE signaling pathway in a PKC-dependent manner. We observed that combined treatment for 24 h with anti-MAG mAb and 50 nM of calphostin, a pharmacological inhibitor of PKC, blocked GSH increase in OLs ($F= 23.63$ $p\leq0.0001$) further confirming this hypothesis (**Figure 3d**). We also confirmed the involvement of Nrf2/ARE signaling pathway on the protective effect of MAG by studying the mRNA expression of genes containing ARE sequences susceptible to the regulation by Nrf2. These included critical enzymes from GSH biosynthesis such as glutathione reductase (GSR), and the catalytic (Gclc) and the regulatory (Gclm) subunits of the glutamate-cysteine ligase, a rate-limiting enzyme in GSH synthesis; as well as the regulatory light chain of system xc- antiporter (xCT). Gene expression was quantified by rtPCR and normalized against the expression of the ribosomal protein l13A (rpl13A). Treatment of OLs with anti-MAG mAb resulted in a significant increase of GSR ($F=29.04$ $p<0.05$), Gclc ($F=25.34$ $p=0.015$), Gclm ($F=53.91$ $p=0.005$) and xCT ($F=24.5$ $p=0.015$) mRNA expression (**Figure 3e**). Increased system xCT protein expression was further confirmed by quantification of immunofluorescence in OL cultures exposed to anti-MAG mAb ($F=5.3$ $p=0.026$) (**Figure 3f and Supplementary Figure 1**). We then quantified the mRNA expression of EAATs, which we previously described to be involved in MAG-mediated Glu uptake. Under similar experimental conditions the analysis of the mRNA expression for Glu transporters GLAST, GLT1 and EAAC1 (mouse homolog's of human EAAT1, 2 and 3 respectively) did not display significant changes at 24 h (data not shown) or at 10 h after anti-MAG treatment (GLT1 $T=0.18$ $p=0.564$, GLAST $T=0.06$ $p=0.708$, EAAC1 $T=0.03$ $p=0.258$) (**Figure 3g**).

MAG activation induces a signaling cascade via phosphoinositides.

PKC activation secondary to MAG activation may be downstream of phospholipase Cγ (PLCγ) activity through the phosphatidylinositol 4,5-bisphosphate (PIP2)/diacylglycerol (DAG) activation pathway. Plasma membrane levels of PIP2 were monitored by transfection of OL cultures with a FRET-based PIP2 biosensor and the FRET efficiency analyzed at different times. Antibody-mediated MAG activation led to a transient increase in PIP_2 (peak at 15 min) (H=12.7 p=0.016), suggesting increased synthesis/recruitment of PIP2 and subsequent degradation to inositol triphosphate and DAG via PLCγ activity (**Figure 4a**). A time course study for DAG using a FRET-based biosensor confirmed an increase in DAG levels starting at 40 min and lasting for at least 60 min after anti-MAG treatment (H= 12.91 p=0.004) coincident with the reduction in PIP_2 levels (**Figure 4b**). Pre-treatment of OL cultures for 1 h with 10 μM U-73122, a pharmacological inhibitor of PLCs, blocked changes in phosphoinositides upon anti-MAG treatment. OLs expressing the PIP_2 biosensor and further exposed to anti-MAG mAb for 60 min after treatment with U-73122 prevented PIP_2 hydrolysis resulting in a net increase of its concentration in plasma membrane (H=12.69 p=0.005) (**Supplementary Figure 2**). Similarly, OLs expressing the DAG biosensor and further treated with U-73122 for 40 minutes did not display an increase in DAG when exposed to anti-MAG mAb (H=9.98 p=0.018) **(Supplementary Figure 2)**. Altogether our results confirm that mAb-mediated activation of MAG results in the stimulation of PLC and subsequent activation of DAG signaling pathways corroborating previous in vitro observations showing binding to and activation of PLCγ by the intracellular portion of MAG (Jaramillo *et al.*, 1994).

Treatment with anti-MAG mAb protects neurons against Glu-mediated toxicity in organotypic cultures.

The ability of MAG activation on OLs to increase Glu uptake and enhance an antioxidant response resulted in protection not only of OLs but also of neighboring cells in the CNS. This was demonstrated using cerebellum organotypic cultures, which conserve their 3D-like architecture and express abundant MAG in oligodendrocytes cell bodies and their myelin process (**Supplementary Figure 3**). Cerebellum slices were cultured for 5 days and then treated for 24 h with anti-MAG mAb or control mAb prior to exposure with 2mM Glu to induce toxicity. The presence of active apoptosis in the cultures was analyzed by confocal microscopy using antibodies against active caspase-3 while granule neurons were identified using anti-NeuN Abs. Treatment with anti-MAG mAb blocked neuronal apoptosis (F=9.93 p=0.001), indicating the protective effect of Glu clearance by OLs in the CNS (**Figure 5**).

Treatment with anti-MAG mAb exerts a neuroprotective effect in a mouse model of Glu-mediated excitotoxicity.

The benefits of anti-MAG treatment have been demonstrated in animal models of stroke, where a mechanism of action involving improvement on axon regeneration has been proposed (Irving *et al.*, 2005; Thompson *et al.*, 2006). However, excitotoxicity plays a major role in disease progression during the first hours post-infarct and different studies identified Glu as target to promote neuroprotection in the "penumbra" area depicting impairment of function (Dirnagl *et al.*, 1999). For this reason, we tested whether in vivo anti-MAG treatment promotes neuroprotection in an acute model of excitotoxicity induced by Glu. Mice (n=16) were cannulated in the striatum and immediately injected with 1 µl of 5 mg/ml anti-MAG mAb or control mAb (n=8 each group). Twenty-four h later, mice received a 0.5 µl injection of 1 M Glu, which saturates the uptake capacity of Glu in the injected area promoting excitotoxic damage (Estrada-Sánchez *et al.*, 2009). Volumetric quantification of Glu-mediated neuronal toxicity was assessed in the striatum 24 h after Glu overload by staining brain with Fluoro Jade C, a specific marker for neurodegeneration. Our data show a strong protective effect of anti-MAG mAb, which lesion volume reduced by ≈60% with respect to mice administered control mAb ($F=12.71$, $p=0.007$) (**Figure 6a**). In a second experiment we tested whether anti-MAG mAb treatment could be beneficial in reducing lesion volumes if administered 1 hr after Glu challenge, an average time in which stroke patients currently received a thrombolytic therapy. Surprisingly, anti-MAG treatment after induction of Glu-toxicity was as effective in reducing lesion volume as the antibody treatment performed prior to Glu administration ($F=7.62$, $p=0.028$) (**Figure 6b**), corroborating the *in vivo* neuroprotective effect of anti-MAG treatment against Glu excitotoxicity.

Treatment with anti-MAG mAb has an axonoprotective effect in a mouse model of experimental autoimmune encephalomyelitis (EAE).

Increasing evidence indicates that altered Glu homeostasis is involved in the pathophysiology of MS (Hohlfeld and Kerschensteiner, 2016), a chronic neurodegenerative inflammatory demyelinating disease of CNS, and high concentration of Glu in spinal fluid is currently proposed as a marker of disease progression (Macrez *et al.*, 2016). Therefore, the potential therapeutic benefit of mAb-mediated MAG activation was tested in a murine model of Experimental Autoimmune Encephalomyelitis (EAE) induced by immunization with a MOG-

derived peptide and characterized by chronic inflammatory demyelination associated with extensive axonal damage (Jones *et al.*, 2008). Treatment consisted of four intraperitoneal injections of 100 μg of anti-MAG mAb (or control mAb) at days 3, 5, 7 and 9 post immunization (n=5 each group). Animals were tested for clinical symptoms of the disease starting a day 10 post immunization using a motor assessment scale. Treatment with anti-MAG mAb delayed onset (+2 days), clinical zenith (+4 days) and significantly reduced clinical symptoms (-0.59 mean clinical score) respect to control mAb-treated animals ($F=3.02$, $p\leq0.0001$) (**Figure 7a**). Morphometric analysis of spinal cord axons showed ≈50% reduction in axon count in control mAb-treated mice when normalized against naive mice (non-EAE) ($F=5.08$, $p=0.025$) (**Figure 7b-d**). In contrast, mice receiving anti-MAG mAb displayed ≈25% reduction in axon counts; however, this difference was not significantly different from non-EAE group (**Figure 7b, e**). We observed a good linear correlation between either the mean clinical score or the highest clinical score and axon count, further highlighting our findings (Pearson correlation values: axon count/mean clinical score P=-0.94; axon count/highest clinical score P=-0.98) (**Figure 7i-J**). Altogether our data are consistent with an *in vivo* axonoprotective role of anti-MAG treatment against Glu toxicity.

Discussion

In recent years, a large body of evidence has uncoupled oligodendroglial functions in axonal support and myelination, clearly demonstrating a protective role of myelin on axons it ensheats (Morrison *et al.*, 2013; Simons and Nave, 2016). One molecule responsible for these effects is MAG, a minor component of the nervous system preferentially expressed on the periaxonal layer of myelinated axons that is involved in bidirectional communication between axons and myelinating cells (Quarles, 2007; Lopez *et al.*, 2011; Lopez, 2014). However, little is known about how signaling generated in axons could have an impact on myelinating cells via MAG. In the nervous system MAG exists predominantly as two isoforms identified as S-MAG (short) and L-MAG (long) that arise from an alternative splicing that produces two proteins with identical extracellular and transmembrane domains but that differ in the length of their cytosolic tails (Lai *et al.* 1987; Salzer *et al.* 1987; Frail and Braun 1984); while the difference in their cytosolic domains is traduced in unique signaling capacities (Kursula *et al.* 1999a, Kursula *et al.* 1999b, Kursula *et al.* 2000, Kursula *et al.* 2001; Jaramillo *et al.* 1994; Umemori *et al.* 1994). MAG expression is regulated temporally and spatially in the nervous system; with L-MAG predominating during CNS development and during myelination whereas S-MAG accumulates at later stages (Inuzuka *et al.* 1991; Ishiguro *et al.* 1991; Tropak *et al.* 1988). Similarly, both isoforms of MAG are expressed in rat OLs cultures (Yim *et al.* 1995). Previous reports have identified that antibody crosslinking-dependent activation of MAG in OLs (using a mAb targeting a conformational epitope located in the extracellular Ig domains 1-3 from MAG triggers specific intracellular signaling events including activation of Fyn kinase, induces cytoskeletal rearrangements, and suggested a protective effect against Glu toxicity (Poltorak *et al.*1987; Meyer-Franke *et al.* 1995; Marta *et al.*, 2004; Irving *et al.*, 2005). Recently, the crystal structure of the extracellular portion of MAG was solved; identifying a symmetry-related dimer maintained via interaction between domains 4 and 5 (Pronker et al. 2016). This was further confirmed by Myllikoski *et al.*, who found that L-MAG dimerize via a high affinity heterotetramer formation between its cytosolic domain with DLC8/DYNLL1 (Myllykoski et al. 2018). Overall, considering the flexibility of the Fab fragments from IgG Abs, it is possible to hypothesize that anti-MAG therapy could exert protection via dimerization of L-MAG and/or stabilization of preassembled L-MAG dimers leading to a multimeric signaling complex in lipids rafts. Whether the anti-MAG mAb favors MAG dimerization through its cytoplasmic domains (dependent or independently from

DLC8) leading to a high avidity docking platform need to be further explored and is beyond the current scope of the manuscript. Also, whether the antibody mimics binding to the neuronal surface or whether MAG activation occurs at the myelin and/or cell body of oligodendrocytes are interesting question that needs further investigation. However, it is important to highlight that circulating anti-MAG Abs (either mAbs or polyclonal) are the pathognomonic feature of a human peripheral neuropathy denominated "anti-MAG neuropathy" characterized by demyelination and loss of node of Ranvier in the presence of an impaired blood nerve barrier; being these findings replicated in experimental models of the disease using passive immunizations with disease-associated and experimental anti-MAG Abs (Dalakas 2008). This is an important question that needs to be further solved. A 150Kd IgG anti-MAG Ab is not able to pass neither the blood brain barrier or access the periaxonal space due to its large size. We hypothesized that in either stroke patients or in experimental models, Abs access the nervous tissue and engage MAG once the initial axonal damage is initiated and permeability/integrity of brain barrier is compromised. *In vivo,* anti-MAG therapy diminished lesion volumes and tissue sparing following middle cerebral artery occlusion (MCAO) and promote functional recovery following experimental traumatic brain injury (Irving *et al.*, 2005; Thompson *et al.*, 2006), but the underlying mechanisms of action remained elusive. In the present study, we identify that antibody-mediated activation of MAG in mature OL cultures triggers the uptake of extracellular Glu, which results in protection against Glu-mediated toxicity to OLs and neighboring cells. Expression of ionotropic and metabotropic Glu receptors is downregulated on mature OLs (Deng *et al.*, 2004; Benarroch, 2009). In addition, mature OLs show resistance to NMDA and AMPA/kainate-mediated toxicity (Wosik *et al.*, 2004; Guo *et al.*, 2012). One of the major causes of Glu-driven OL toxicity and death is oxidative stress as a result of inhibition of cystine import that leads to GSH depletion (Oka *et al.*, 1993; Rosin *et al.*, 2004; Irving *et al.*, 2005). System xc- and Glu transporters are known to work synergistically in order to increase intracellular GSH, the major antioxidant in the mammalian CNS (Lewerenz *et al.*, 2006), by increasing intracellular concentrations of its metabolic precursors Glu and cysteine. Interestingly, activation of MAG raised GSH levels in OLs in a system xc- and EAAT-dependent manner. The transcription factor Nrf2 plays a central role linking MAG activation with the initiation of antioxidant responses. We observed that mAb-mediated MAG activation increased nuclear Nrf2-ser40 levels in a PKC-dependent manner through activation of phosphoinositide signaling pathways. Moreover, anti-MAG treatment of OLs enhanced the mRNA expression of xCT, the regulatory subunit chain of system xc-, as well as critical enzymes from GSH biosynthesis, all bearing the ARE consensus sequence recognized by Nrf2, while not affecting EAATs expression. Overall, MAG activation exerted protection of OLs by

modulating highly toxic extracellular Glu concentrations, an effect achieved through increased Glu uptake via EAATs and its further release through antiporter System xc-. Glu recycling through the plasma membrane of OLs increases the supply of intracellular cysteine and Glu required for the first step of GSH biosynthesis, which is further boosted by increased expression of its rate-limiting enzyme. An open question remains as to whether this mechanism accounts for the protection observed on neurons after anti-MAG mAb treatment in *in vivo* paradigms. It has been described that oligodendroglial exosomes can protect neurons from oxidative stress (Frühbeis *et al.*, 2013). As GSH is consistently higher in glia than in neuronal cells (Chatterjee *et al.*, 1999), it is possible to speculate that anti-MAG stimulated OLs could protect neurons via exporting GSH through exosomes.

Recently, the anti-MAG mAb used in this study has been humanized (GSK249320), modified to reduce potential interactions with the human immune system, and its efficacy tested in stroke patients (Cramer *et al.*, 2013, 2017). Based on the success observed in different preclinical studies (Barbay *et al.*, 2015; Cash *et al.*, 2016), it is proposed that anti-MAG therapy should promote clinical recovery by blocking the inhibitory activity of MAG on axon regeneration, therefore allowing functional recovery in the CNS. However, despite ruling out a toxic effect of this mAb in human healthy volunteers (Abila *et al.*, 2013), anti-MAG treatment failed to succeed as a restorative therapy in patients with Stroke. The question then arises as to why anti-MAG treatment in humans did not reproduce the preclinical effects. Although animal models may not accurately reflect the complex scenario observed in stroke patients, it could be argued that the proposed mechanisms of actions for the anti-MAG treatment have not been well documented. First, despite extensive research, the inhibitory role of MAG on axon regeneration *in vivo* has not been convincingly demonstrated (Lee *et al.*, 2010). Secondly, preclinical studies do not conclusively support the concept of increased axon regeneration but rather evidence a neuroprotective mechanism (e.g. significant reduction of lesion volumes and motor function improvement as soon as 24 h after lesion in the MCAO model in the absence of increased sprouting in the lesioned area 7 days post-injury) (Irving *et al.*, 2005; Thompson *et al.*, 2006; McKerracher and Rosen, 2015). Our results confirm the neuroprotective effect of anti-MAG therapy in a model of excitotoxicity induced by intracranial delivery of Glu (reduction of lesion volumes at 24 h), clearly demonstrating neuronal protection against Glu overload by OLs. Animal models of stroke such as MCAO support the notion of Glu-mediated excitotoxicity as the main pathophysiological mechanism during the first hours of clinical onset (Dirnagl *et al.*, 1999). However, in stroke patients anti-MAG therapy was administered intravenously within the first 72

h after the initiation of clinical symptoms. Although the therapy failed to promote clinical improvement, a trend toward improvement of gait velocity was reported in these patients (Cramer *et al.*, 2013, 2017). One can speculate that the efficacy of anti-MAG therapy in human clinical trials failed due to a delayed treatment that impeded Glu reuptake before it caused significant damage. If so, our data provide evidence to revise the clinical protocols in order to improve the efficacy of anti-MAG mAb for treatment of stroke.

Another important clinical derivation of our results is the further understanding of the pathophysiological mechanisms of Glu-mediated neurodegenerative processes associated with demyelinating diseases. One such example is the human disease MS, a chronic degenerative disease of the CNS in which Glu overload plays a central role on pathology and where virtually all aspects of glutamate homeostasis are pathologically altered (Kostic *et al.*, 2013). In MS patients, high Glu concentrations generated by infiltrating macrophages and microglial cells correlate with clinical disability (Pampliega *et al.*, 2011; Hohlfeld and Kerschensteiner, 2016; Macrez *et al.*, 2016). Moreover, multivoxel spectroscopy in 343 MS patients demonstrated that high Glu concentrations correlated with the rate of decline of brain volume loss, MSFC, and PASAT in affected patients finding a clinical correlation between Glu and disease progression (Azevedo *et al.*, 2014). Key enzymes of Glu metabolism and Glu transporters are present predominantly on OLs and to a much lesser extent on astrocytes, suggesting that OLs contribute to maintain Glu homeostasis in white matter (Werner *et al.*, 2001; Haroon *et al.*, 2017). Also, the relative lack of Glu transporters, especially EAAT 2, in astrocytes from white matter places OLs in a key position for maintaining Glu homeostasis (Pitt *et al.*, 2003). MR spectroscopy analysis in MS lesions detected high levels of Glu in normal appearing white matter and active plaques of demyelination showing axonal damage; while there is evidence of altered Glu homeostasis by OLs (Macrez *et al.*, 2016). Interestingly, there is a reduced expression of MAG in the acute phase of active plaque formation (Stys *et al.*, 2012). The dysfunction or loss of OLs that characterizes MS could reduce the ability of white matter to uptake Glu, resulting in Glu toxicity on neurons and glial cells. We tested the efficacy of anti-MAG mAb in the EAE model showing demyelination associated with extensive axonal damage, where it was reported that treatment with AMPA/kainite antagonists results in substantial disease amelioration, by reducing axonal damage and increasing OLs survival (Pitt *et al.*, 2000; Smith *et al.*, 2000). Anti-MAG therapy initiated before the acute phase of axon degeneration and lasting until first clinical symptoms demonstrated efficacy in delaying clinical onset, reduced maximal clinical scores and reduced the extent of axonal damage in the spinal cord. Interestingly, increased axonal loss in an EAE model was found in

MAG-null mice, which was interpreted as a lost of the direct axonoprotective properties of MAG on axons (Jones *et al.*, 2013). However, anti-MAG therapy, which blocks MAG interactions with its axonal receptors, resulted in axonoprotection, further supporting the concept of a protective role of OLs via MAG activation. Altogether, anti-MAG therapy appears as a promising treatment to mitigate disease progression in chronic forms of MS characterized by axonal atrophy.

Overall, a new mechanism of oligodendroglial protection against Glu toxicity driven by MAG activation was discovered. These studies add knowledge to the function of MAG in OLs and also describe the molecular mechanisms underlying anti-MAG mAb therapy, distinct from axon growth promotion. Its participation in regulating extracellular Glu concentrations and Glu metabolism as well as increasing anti-oxidative defenses place MAG as a promising therapeutic target to mitigate the devastating consequences of Glu toxicity in the CNS. Mechanisms of action, signaling pathways and timing insights could help guide precise clinical trials to fight MS and stroke.

Materials and Methods

1. Primary OL cultures.

Mature primary OL cultures were established by in vitro differentiation of OLs progenitor cells (OPCs) isolated from new born rats as described (Mecha, 2011), with some minor modifications. Briefly, forebrains of P0-P2 neonatal pups were harvested in DMEM. After meningeal removal, tissues were mechanically dissociated and cells pellet by centrifugation, resuspended in growth media (DMEM/F12, 10% normal horse serum (NHS), 1% glutamine, 15mM glucose, and 1% pen/strep) and seeded on poly-D-lysine coated 75 cm^2 tissue culture flasks. After 11 days of culture (37ºC, 5% CO2), OPCs were detached by overnight shaking at 260 rpm. Filtered cell suspension (40 µm nylon mesh) was transferred to a petri dish and non-adherent cells collected after 24 h by centrifugation at 1000 rpm x 10 min. OPCs were seeded dropwise on each 12mm poly-D-lysine-coated glass coverslips, at 50.000 cells/coverslip. Media was replaced within 1:30 h. with freshly-prepared OLs differentiation media (DMEM/F12, 1% N1 supplement, 1% glutamax, 15 mM glucose,1% fetal bovine serum, 1% pen/strep, 10 nM biotin, 5 ng/ml PDGF-AA, and 5 ng/ml bFGF). Growth factors were depleted 2 days after plating and cells were further cultured for 4 days to obtain mature OLs.

2. Cerebellar organotypic cultures

Cerebella were removed from 7-day old rat pups and placed on ice-cold dissection media (HBSS, 4.3mM sodium bicarbonate, 10mM Hepes, 33.3mM D-glucose, 5.8mM magnesium sulfate, 0.03% bovine serum albumin and (1%) pen/strep and sectioned (250 µm) using a tissue chopper. Sections were transferred onto cell culture inserts (millicell-PCF 0.4 µm, Millipore, USA) and cultured for a week in media consisting of 50% DMEM supplemented with 25% HBSS, 25% NHS, 25 mM Hepes, 35 mM D-glucose, 2 mM glutamine and 1X pen/strep. Cultures were maintained for 4 days at 37°C in a 5% CO_2 incubator until treatment.

3. Culture treatment

Anti-MAG monoclonal antibody (Millipore Cat# MAB1567 RRID:AB_2137847, named anti-MAG mAb) (Poltorak *et al.*, 1987; Meyer-Franke *et al.* 1995) and its isotype control anti-C-Myc (DSHB Cat# 9E10, RRID:AB_2266850) were generated from their hybridoma. Dosage of anti-MAG treatment (2 µg/ml) was based on a previous report showing protection of OLs against Glu toxicity (Irving *et al.*, 2005). To induce Glu toxicity, 8.6 mg/ml L-Glutamic-acid was dissolved

in DMEM and used at a final concentration of 2 mM. Based in a pilot dose-response curve we set the concentration of xCT inhibitor L-2 Aminoadipic acid (AAA) as 0.6 mM which was effective without affecting OLs viability. Glu transporter inhibitor L-trans-pyrrolidine-2,4-dicarboxilic acid (PDC) was used at a concentration of 300 µM and selective PKC inhibitor Calphostin-C was used 50 nM as described elsewhere (Baron *et al.*, 2000; DeSilva *et al.*, 2009). PLC inhibitor U-73122 was used at 10 µM concentration, based on activity range previously described in OLs (Deng *et al.*, 2004; Gudz, 2006). All inhibitors were applied 60 min before antibody.

4. Glutathione analysis

Analysis of intracellular GSH content in primary OL cultures was determined by using Monochlorobimane (mBCl) (Keelan *et al.*, 2001)**.** Cultures were treated with 60 mM mBCl for 20 min and then fixed with 4% Paraformaldehyde (PFA) and 0.2% glutaraldehyde for 10 min, further counterstained with the mature OL marker C4 (to delineate OLs cell bodies and processes), and examined under fluorescence microscopy. Mean fluorescent intensities of mBCl in OLs bodies were calculated using Fiji software using raw images.

5. FRET analysis

5.1 Glutamate biosensors

Relative Glu quantification in OLs was determined by using FRET-based biosensors as described (Okumoto *et al.*, 2005). Plasmids pDisplay FLIPE-1m and pcDNA3.1 FLIPE-10u (#13548 and #13542, Addgene, USA) were used to monitor extracellular and intracellular Glu changes, respectively. This family of biosensors display FRET activity under control condition (no glutamate) and respond with different affinities to glutamate exposure (1M for FLIPE-1m and 10µM for FLIPE-10u) by reducing FRET activity proportionally to its concentration. Plasmids were transfected using lipofectamine 2000 (Thermo Fisher Scientific, USA) and OLs were culture for 24 h to allow their expression. Then OLs were treated with control or anti-MAG mAb as described above for additional 24 h before being challenged with 2 Glu at different times. Then OL cultures were fixed with 4% PFA, mounted and processed for radiometric FRET map calculation. These sensors respond to Glu with a reversible concentration-dependent decrease in FRET efficiency. Images were acquired with either a Spinning Disk Olympus DSU microscope (60 x m 1.42 NA immersion objective) (for extracellular Glu) or an Olympus Fluoview 1000 spectral microscope (60 x m 1.42 NA immersion objective) (intracellular Glu) and images processed as described (Palandri *et al.*, 2015). Briefly, CFP and YFP images were acquired while exciting the donor. The following filter sets were used: 457 and 514 nm Argon multiline laser of 40 mw

model 35-IMA 040-220 of CVI MellesGriot. Fiji software was used to perform image analysis. All images were first drift-corrected and background-subtracted. FRET image, that has the largest signal-to-noise ratio and therefore provides the best distinction between the cell and the background, was thresholded to generate a binary mask with a value of zero outside the cell and a value of one inside the cell. After multiplication by this mask, the FRET image was divided by the CFP image to yield a ratio image reflecting glutamate presence on OLs.

5.2 PLC activation analysis

PLC activation in OLs was determined by using two FRET-based biosensors that recognize either its substrate (phosphatidylinositol 4,5-bisphosphate (PIP2), Frubby biosensor (Mavrantoni *et al.*, 2015) or its enzyme product diacylglycerol (DAG), DIGDA biosensor (Nishioka *et al.*, 2008). Plasmids were kindly provided by Dr. Halaszovich, Philipps-Universität-Marburg, Germany. OLs were transfected with FRET sensors for 24 h, and then exposed to control mAb or anti-MAG mAb as described above. Confocal images were taken with an Olympus Fluoview-1000 spectral microscope as previously described (Palandri *et al.*, 2015). Once the FRET/CFP ratio was obtained, FRET efficiency in OLs plasma membrane was determined in a linear 4-pixel-wide ROI selection that includes the cell membrane and five random equidistant processes (distant 10 µm from soma) using Fiji software at different time points.

6. Quantification of extracellular Glutamate

Extracellular Glu was measured by fluorimetry of NADH generated by exogenous glutamate dehydrogenase (Sigma) as described (Chanaday *et. al*, 2015). Media from mature OLs cultures treated for 24 h with IgG or anti-MAG (2µg/ml) and further exposed to 2mM Glu for 1h or 24h were collected for extracellular Glu determination. Media were diluted in PBS and 1mM NAD+ and 25 units/ml glutamate dehydrogenase were added to a final volume of 200µl. The mix was incubated in a thermostated cuvette maintained at 37 °C in an ISS Chronos fluorescence lifetime spectrometer (Champaign, IL, USA). After 10 min of incubation, NADH production was measured at 450nm (using an excitation of 350nm). A calibration curve with different glutamate concentrations (ranging from 5µM to 200 µM) was used to calculate the extracellular glutamate concentration.

7. Nrf2 and xCT expression analysis

The active form of Nrf2 (phosphorylated at serine 40, Nrf2-ser40) was quantified in OL cultures by double-labeled immunofluorescence using specific Abs for Nrf2-ser40 (Bioss Inc Cat# bs-2013R, RRID:AB_10855428) and MAG (anti-MAG mAb) and further 2-(4-Amidinophenyl)-6-

indolecarbamidine dihydrochloride (Dapi) counterstain. OLs were imaged using confocal microscopy and the nuclear translocation/activation of Nrf2-ser-40 determined by scanning the whole cell volume using 1µm depth steps. Z projection of the Nrf2-ser40 channel stack was obtained using Fiji software. In MAG positive cells, a ROI delineating the nuclei was created using the Dapi channel and used on collapsed Nrf2-ser-40 images to obtain the mean intensity value of nuclear translocation. Surface expression of xCT in OLs was carried out in a similar manner. Mean fluorescence intensities of Z projection of 1µm confocal slices were analyzed using a ROI for OLs soma and processes.

8. rtPCR

Total RNA was extracted from OL cultures using Trizol (Thermo Fisher Scientific) isolated according to manufacturer's protocol and further treated with DNAse I. Reverse transciption reactions (using 1.5 µg of RNA) were performed using a commercially available kit (Superscript III First-Strand Synthesis System, Invitrogen) with random hexamers. Primer sets were designed using Primer3plus software (RRID:SCR_003139), allowing specific amplification of Rattus norvegicus Glutathione reductase, system xCT, catalytic and modulatory subunits of Glu-cysteine ligase, Glu transporter GLAST, GLT1 and EAAC1. We chose Ribosomal protein l13a (Rpl13a) as the housekeeping gene according with previous comparative work of housekeeping genes suitable for OL cultures (Nelissen et al., 2010). All primers sets are shown in Supplementary Table 1. rtPCR was performed in an optical 48-well plate (Applied Biosystems, USA) with Step OneTM Real Time PCR System (Applied Biosystems) and universal cycling conditions (10 min a 95 °C, 40 cycles of 15 s at 95 °C and 60 s at 60 °C). Each 15 µl reaction contained 1X SYBR Green Master Mix (Applied Biosystems), 400 nM gene-specific forward and reverse primers, 1X nuclease-free water and pre-diluted cDNA. Primer efficiency was determined by a standard curve of 1:3 serial dilutions starting from pure cDNA. CT values of the samples are positioned within the dynamic linear range of the calibration curve. Amplification was followed by a melting curve analysis to check PCR product specificity and primer dimers absence. Data were analyzed using the ΔΔCt method (Livak and Schmittgen, 2001). mRNA expression levels and associated errors were calculated as described by manufacturer instructions (Applied Biosystems User Bulletin).

9. HyPer analysis

OL cultures were transfected with a mammalian expression vector encoding mitochondria-

targeted HyPer (pHyPer-dMito, cat FP942, evrogen). Upon treatment with Abs, OLs were fixed and cultures were excited at 488 and 405nm. The emission was collected at 500-520 nm wavelength range in both cases. Fluorescence emission from excitation at 488 nm was divided by fluorescence emission at 405nm excitation (488:405), as a measure of H_2O_2 content (Belousov *et al.*, 2006). To generate a H_2O_2 map, the ratio 488:405 was divided by the binary mask of OL mitochondria. Images were acquired using a Olympus-FV1000 confocal microscope using a 60X oil/1.4 N.A. objective.

10. TMRE analysis

To assess mitochondrial potential, primary OL cultures were plated into 25 mm rounded glass coverslips at a density of 100,000 cells/coverslip. After differentiation into mature OLs, cultures were treated with anti-MAG mAb (2 µg/ml) or control IgG. 24 hours after antibody treatment, cultures were treated with 2mM Glu. OL mitochondrial membrane potential was measured at 24 hours after Glu treatment by incubating cultures with tetramethylrhodamine (TMRE), a live dye mitochondrial potential probe (Thermofisher T669, final concentration 10nM) in DMEM-F12 for 10 minutes. After incubation, media was replaced with OL differentiation media without phenol red and cells were imaged using a Spinning Disk Olympus DSU microscope, with a 60 ×/1.42 NA immersion objective, Ex/Em: 549/575 and 1um steps. At least 15 image stacks were obtained per condition and all conditions were repeated 3 times. Stacks were processed using Fiji Software. The mean intensity of each cell was obtained using a maximum projection of stacks and a threshold for mitochondria.

11. Animal Models

All of the reported experimental protocols developed at Instituto de Investigación Médica Mercedes y Martin Ferreyra-INIMEC-CONICET-Universidad Nacional de Córdoba were approved by the appropriate animal care and use committees at our institute, following the National Institutes of Health guidelines for the care and use of laboratory animals. Treatments were randomly administered among animals and all cages contained animals with different treatments. The investigators were blind to the treatment assignments.

11.1 Excitotoxicity model

11.1.1 Surgery

Twelve week-old C57Bl/6 male mice were anesthetized with ketamine and xilazine (90 mg/kg and 10 mg/Kg, respectively) and placed on a rat stereotaxic frame with a mouse adapter; a cannula was positioned near the left striatum (coordinates AP + 0.8 mm, L -1.5 and V −1.2) according to the mouse brain atlas (Franklin and Paxinos, 2008). Antibody administration was carried out in two different ways. On the pre-lesion treatment, mice were anesthetized with isofluorane after 48 h of surgery recovery, and either control mAb or anti-MAG mAb (1µl, 5µg/µl, 1µl/min) were injected into the left striatum using a 30G (AP +0.8 mm, L -1.5 and V −3.2). Five min after the injection, the needle was gently withdrawn. 24 h later, the same procedure was used to inject Glu solubilized in distilled water. A dose of 500 nmol of Glu in 0.5 µl was selected based on literature indicating as an effective dose to generate a significant lesion in striatum (Estrada-Sánchez *et al.*, 2009). In the post-lesion treatment, similar dose of Abs were injected 1 h after Glu challenge. Mice were allowed to recover from anesthesia and placed in individual cages with water and food *ad libitum*.

11.1.2 Histology, Fluoro Jade C, and lesion volume quantification

Twenty-four h after intrastriatal injection of Glu, mice were anesthetized with isofluorane and transcardially perfused with 4% PFA. Brains immediately removed and postfixed overnight and further cryoprotected. Brains were embedded in Tissue-Tek® O.C.T. (Sakura Finetek, USA) and consecutive series of 40 µm cryostat coronal sections from striatum obtained and mounted in gelatin-coated glass slides. For lesion volume reconstruction and analysis, 120µm-spaced serial brain sections were stained with Fluoro Jade C (FJC) as described (Schmued *et al.*, 2005). Damaged brain areas (FJC+) were obtained using an epifluorescence microscope. For each slice, 40x photomicrographs were taken, merged and analyzed with Fiji software (RRID:SCR_002285) using Volumest, a volume calculator plug-in.

12. Experimental Autoimmune Encephalomyelitis

12.1. Two months old male C57BL/6 mice maintained in a pathogen-free environment were immunized subcutaneously at the tail base with 100µl of mouse $MOG_{35–55}$-derivedpeptide (NH2-MEVGWYRSPFSRVVHLYRNGK-COOH; synthesized at the Synthesis & Sequencing Core Facility-JHU, Baltimore, MD) emulsified in complete Freund's adjuvant (CFA) supplemented with 8 mg/ml of heat-killed *Mycobacterium tuberculosis* (H37 RA; Difco-BD, Sparks, MD). Pertussis toxin (250 ng; Calbiochem, Gibbstown, NJ) was injected intravenously on the day of immunization and again two days later. Mice were assessed daily for clinical evidence of the

disease and their motor performance scored at 10 days post-immunization. Motor assessment scoring was as follows (Jones *et al.*, 2008): 0, no deficit; 0.5, partial loss of tail tone or slightly abnormal gait; 1.0, complete tail paralysis or both partial loss of tail tone and mild hind limb weakness; 1.5, complete tail paralysis and mild hind limb weakness; 2.0: tail paralysis with moderate hind limb weakness (evidenced by frequent foot dropping between bars of cage top while walking); 2.5, no weight-bearing on hind limbs (dragging) but with some leg movement; 3.0, complete hind limb paralysis with no residual movement; 3.5, hind limb paralysis with mild weakness in forelimbs; 4.0, complete quadriplegia but with some movement of head; 4.5, moribund; 5.0, dead. Fractional scores result either from calculating the mean of scores from a group of animals or from assigning fractional scores for partial but distinct phenotypes; for example, when the distal tail droops while the tail can be raised overall, a score of 0.5 is assigned and when one leg is dragging but the other bears a large fraction of the body's weight (allowing the mouse to actually walk), a score of 2.5 or 2.75 (between 2.0 for one leg and 2.5 or 3.0 for the other) is assigned.

12.2. Axon counting

After 30 days post-immunization, mice were anesthetized with an overdose of isoflurane and perfused with 4% PFA and 2.5 % glutaraldehyde. The spinal columns were postfixed overnight at 4°C, then C3-C5 cervical sections isolated and further fixed with 1% osmium tetraoxide and embedded in Epoxipropyl ether of glycerol. Semi-thin 1µm sections of C5 spinal segments were cut and stained with toluidine blue, and further imaged using a light microscope (Zeiss, Jena, Germany) equipped with a Leica LC200 video camera (Heerbrugg, Switzerland) x 40 magnification, 1.42 NA air objective were merged to reconstitute the dorsal column and adjacent areas. The axons in the medial dorsal column on the spinal cord at C5 were manually quantified. The dorsal columns are reproducibly damaged in this model of EAE (though the rostral–caudal level of damage was less predictable) and C5 was chosen to include ascending fibers from both the upper and lower limbs in the count (Jones *et al.*, 2008). Using Fiji software an inverted triangular ROI was drawn within the gracile fasciculus: a line from the spinal canal to the dorsal surface was bisected to indicate the dorsal half of the column (height of the triangle) and a line perpendicular to this was drawn on both sides from the most medial part of the column to the ends of gracile fasciculus on the dorsal surface as described (Nguyen *et al.*, 2009). Axon count was performed using cell counter plugin for Fiji. Only clearly visible, intact, myelinated axons > 1µm diameter were included.

13. Immunofluorescence.

Organotypic cultures were fixed for 1 h in 4% PFA and washed three times with PBS. After antibody retrieval (10mM Sodium Citrate 0.05% Tween-20 pH 6 at 60ºC for 30 min) cultures were incubated for 6 h at RT with blocking solution (1mmol/L HEPES, 2% NHS, 10% FBS, 1% BSA, 0.25% Triton x-100 in HBSS). Primary antibodies (anti-NeuN, Millipore Cat# MAB377 RRID:AB_2298772, 1:1000, anti-cleaved caspase-3, 1:500, Cell Signaling Cat 9661 RRID:AB_2341188) were added in blocking solution. After 48 h of incubation at 4 °C, cultures were washed 3 times in PBS and incubated with secondary antibodies (Alexa Fluor 488-Donkey Anti-Rabbit, 1:1000, Cy3-Donkey Anti-Mouse, 1:1000; Jackson Immunoresearch Laboratories) in PBS for 24 h at 4°C and then incubated with Dapi 3µM, washed and mounted in Mowiol® 4-88 (SIGMA, USA). Primary OL cultures were fixed for 20 min at 37°C in 4% PFA and permeabilized 10 min with 0.2% Triton X-100. Permeabilization steps were omitted when studying membrane proteins. After incubation with blocking solution (10% NHS in PBS) for 1 h, OLs were incubated with primary antibodies (anti-O4, Neuromics, MO15002, 1:500, anti x-CT, Abcam, ab60171, 1:500, anti-Ser-40-Nrf2, Bioss bs-2013R, 1:200, anti-MAG mAb clone 513, 1:300) overnight in 5% NHS in PBS at 4º C. Then cultures were incubated with secondary antibodies (Cy3-donkey anti-mouse, 1:1000; Alexa Fluor 488-donkey anti Mouse, Cy3-donkey anti-Rabbit, 1:1000, Alexa Fluor donkey anti-Goat, 1:1000; JIL) for 1 h at RT in blocking buffer (PBS, 5% NHS, 0.1% Triton X-100) for 2 h and then mounted with Mowiol® 4-88.

14. Statistical Analyses

All in vitro experiments were carried out three times on independent conditions. All values are shown as the mean ± SEM. Data analysis was performed using standard statistical packages (InfoStat software, RRID:SCR_014310) in all experiments. The investigators quantifying images were blind to the treatment assignments. All the data sets were tested for normal distribution and variance homogeneity. Normally distributed data was analyzed by Student's t-test or one-way analysis of variance (ANOVA) followed by David Garcia-Callejas (DGC) post hoc test. Non-parametric distribution data sets were analyzed with Kruskal-Wallis test.

References

Abila B, Cunningham E, Simeoni M. (2013). First-Time-in-Human Study With GSK249320, a Myelin-Associated Glycoprotein Inhibitor, in Healthy Volunteers. Clinical Pharmacology & Therapeutics, 93, 163–169.

Azevedo CJ, Kornak J, Chu P, Sampat M, Okuda DT, Cree BA, Nelson SJ, Hauser SL, Pelletier D. (2014). In vivo evidence of glutamate toxicity in multiple sclerosis. Annals Neurology., 76(2), 269-278.

Barbay S, Plautz EJ, Zoubina E, Frost SB, Cramer SC, Nudo RJ. (2015). Effects of Postinfarct Myelin-Associated Glycoprotein Antibody Treatment on Motor Recovery and Motor Map Plasticity in Squirrel Monkeys. Stroke, 46, 1620–1625.

Baron W, Metz B, Bansal R, Hoekstra D, de Vries H. (2000). PDGF and FGF-2 Signaling in Oligodendrocyte Progenitor Cells: Regulation of Proliferation and Differentiation by Multiple Intracellular Signaling Pathways. Molecular and Cellular Neurosciences, 15, 314–329.

Belousov VV, Fradkov AF, Lukyanov KA, Staroverov DB, Shakhbazov KS, Terskikh AV, *et al.* (2006). Genetically encoded fluorescent indicator for intracellular hydrogen peroxide. Nature Methods, 3, 281–286.

Benarroch EE. Oligodendrocytes: Susceptibility to injury and involvement in neurologic disease. (2009). Neurology, 72, 1779–1785.

Bloom DA, Jaiswal AK. (2003). Phosphorylation of Nrf2 at Ser40 by protein kinase C in response to antioxidants leads to the release of Nrf2 from INrf2, but is not required for Nrf2 stabilization/accumulation in the nucleus and transcriptional activation of antioxidant response element-mediated NAD(P)H:quinone oxidoreductase-1 gene expression. Journal of Biological Chemistry, 278, 44675–44682.

Cash D, Easton AC, Mesquita M, Beech J, Williams S, Lloyd A, *et al.* (2016). GSK249320, A Monoclonal Antibody Against the Axon Outgrowth Inhibition Molecule Myelin-Associated

Glycoprotein, Improves Outcome of Rodents with Experimental Stroke. Journal of Neurology and Experimental Neurocience, 2, 28–33.

Chanaday NL, Vilcaes AA, de Paul AL, Torres AI, Degano AL, Roth GA (2015). Glutamate release machinery is altered in the frontal cortex of rats with experimental autoimmune encephalomyelitis. Mol Neurobiol. 2015;51(3):1353-67.

Chatterjee S, Noack H, Possel H, Keilhoff G, Wolf G. (1999) Glutathione levels in primary glial cultures: Monochlorobimane provides evidence of cell type-specific distribution. Glia, 27, 152–161.

Cramer SC, Abila B, Scott NE, Simeoni M, Enney LA, MAG111539 Study Investigators. (2013). Safety, pharmacokinetics, and pharmacodynamics of escalating repeat doses of GSK249320 in patients with stroke. Stroke, 44, 1337–1342.

Cramer SC, Enney LA, Russell CK, Simeoni M, Thompson TR. (2017). Proof-of-Concept Randomized Trial of the Monoclonal Antibody GSK249320 Versus Placebo in Stroke Patients. Stroke, 48, 692–698.

Dalakas MC (2018). Advances in the diagnosis, immunopathogenesis and therapies of IgM-anti-MAG antibody-mediated neuropathies. Ther Adv Neurol Disord.;11:1756285617746640.

Deng W, Wang H, Rosenberg PA, Volpe JJ, Jensen FE. (2004). Role of metabotropic glutamate receptors in oligodendrocyte excitotoxicity and oxidative stress. Proceedings of the National Academy of Sciences U. S. A., 101, 7751–7756.

DeSilva TM, Kabakov AY, Goldhoff PE, Volpe JJ, Rosenberg PA. (2009). Regulation of Glutamate Transport in Developing Rat Oligodendrocytes. Journal Neuroscience, 29, 7898–7908.

Dirnagl U, Iadecola C, Moskowitz MA. (1999). Pathobiology of ischaemic stroke: an integrated view. Trends in Neurosciences., 22, 391–397.

Estrada-Sánchez AM, Montiel T, Segovia J, Massieu L. (2009). Glutamate toxicity in the striatum of the R6/2 Huntington's disease transgenic mice is age-dependent and correlates with decreased levels of glutamate transporters. Neurobiology of Disease, 34, 78–86.

Frail DE, Braun PE (1984). Two developmentally regulated messenger RNAs differing in their coding region may exist for the myelin-associated glycoprotein. J Biol Chem; 259(23):14857-62.

Franklin KBJ, Paxinos G. (2008). The mouse brain in stereotaxic coordinates. Amsterdam: Boston: Elsevier/Academic Press.

Frühbeis C, Fröhlich D, Kuo WP, Amphornrat J, Thilemann S, Saab AS, *et al.* (2013). Neurotransmitter-Triggered Transfer of Exosomes Mediates Oligodendrocyte–Neuron Communication. PLoS Biology, 11, e1001604.

Gudz TI. (2006) Glutamate Stimulates Oligodendrocyte Progenitor Migration Mediated via an v Integrin/Myelin Proteolipid Protein Complex. Journal Neuroscience, 26, 2458–2466.

Guo F, Maeda Y, Ko EM, Delgado M, Horiuchi M, Soulika A, *et al.* (2012). Disruption of NMDA Receptors in Oligodendroglial Lineage Cells Does Not Alter Their Susceptibility to Experimental Autoimmune Encephalomyelitis or Their Normal Development. Journal Neuroscience, 32, 639–645.

Haroon E, Miller AH, Sanacora G. (2017). Inflammation, Glutamate, and Glia: A Trio of Trouble in Mood Disorders. Neuropsychopharmacology, 42, 193–215.

Hohlfeld R, Kerschensteiner M. (2016). Antiglutamatergic therapy for multiple sclerosis? Lancet Neurology, 15, 1003–1004.

Huang H-C, Nguyen T, Pickett CB. (2002). Phosphorylation of Nrf2 at Ser-40 by protein kinase C regulates antioxidant response element-mediated transcription. Journal of Biological Chemistry, 277, 42769–42774.

Inuzuka T, Fujita N, Sato S, Baba H, Nakano R, Ishiguro H, *et al.* (1991). Expression of the large myelin-associated glycoprotein isoform during the development in the mouse peripheral nervous system. Brain Res;562(1):173-5.

Irving EA, Vinson M, Rosin C, Roberts JC, Chapman DM, Facci L, *et al.* (2005).

Identification of neuroprotective properties of anti-MAG antibody: a novel approach for the treatment of stroke? Journal of Cerebral Blood Flow & Metabolism, 25, 98–107.

Ishiguro H, Sato S, Fujita N, Inuzuka T, Nakano R, Miyatake T (1991). Immunohistochemical localization of myelin-associated glycoprotein isoforms during the development in the mouse brain. Brain Res;563(1-2):288-92.

Jaramillo ML, Afar DE, Almazan G, Bell JC. (1994). Identification of tyrosine 620 as the major phosphorylation site of myelin-associated glycoprotein and its implication in interacting with signaling molecules. Journal of Biological Chemistry, 269, 27240–27245.

Jones MV, Nguyen TT, Deboy CA, Griffin JW, Whartenby KA, Kerr DA, *et al.* (2008). Behavioral and pathological outcomes in MOG 35-55 experimental autoimmune encephalomyelitis. Journal of Neuroimmunology, 199, 83–93.

Jones MV, Nguyen TT, Ewaleifoh O, Lebson L, Whartenby KA, Griffin JW, *et al.* (2013) Accelerated axon loss in MOG35-55 experimental autoimmune encephalomyelitis (EAE) in myelin-associated glycoprotein-deficient (MAGKO) mice. Journal of Neuroimmunology, 262, 53–61.

Keelan J, Allen NJ, Antcliffe D, Pal S, Duchen MR. (2001). Quantitative imaging of glutathione in hippocampal neurons and glia in culture using monochlorobimane. Journal of Neuroscience Research, 66, 873–884.

Kirchhoff F, Hofer H-W, Schachner M. (1993). Myelin-associated glycoprotein is phosphorylated by protein kinase C. Journal of Neuroscience Research, 36, 368–381.

Kostic M, Zivkovic N, Stojanovic I. (2013). Multiple sclerosis and glutamate excitotoxicity. Reviews in Neurosciences., 24, 71–88.

Kumari S, Mehta SL, Li PA (2012). Glutamate induces mitochondrial dynamic imbalance and autophagy activation: preventive effects of selenium. PLoS One; 7(6):e39382.

Kursula P, Merilainen G, Lehto VP, Heape AM (1999a). The small myelin-associated glycoprotein is

a zinc-binding protein. J Neurochem ;73(5):2110-8

Kursula P, Tikkanen G, Lehto VP, Nishikimi M, Heape AM (1999b). Calcium-dependent interaction between the large myelin-associated glycoprotein and S100beta. J Neurochem;73(4):1724-32.

Kursula P, Lehto VP, Heape AM (2000). S100beta inhibits the phosphorylation of the L-MAG cytoplasmic domain by PKA. Brain Res Mol Brain Res;76(2):407-10.

Kursula P, Lehto VP, Heape AM (2001). The small myelin-associated glycoprotein binds to tubulin and microtubules. Brain Res Mol Brain Res;87(1):22-30.

Lau A, Tian W, Whitman SA, Zhang DD. (2013) The predicted molecular weight of Nrf2: it is what it is not. Antioxid Redox Signal 1;18(1):91-3.

Lai C, Brow MA, Nave KA, Noronha AB, Quarles RF, Bloom FE, *et al.* (1987). Two forms of 1B236/myelin associated glycoprotein, a cell adhesion molecule for postnatal neural development, are
produced by alternative splicing. Proc Natl Acad Sci U S A Jun;84(12):4337-41.

Lee JK, Geoffroy CG, Chan AF, Tolentino KE, Crawford MJ, Leal MA, *et al.* (2010). Assessing Spinal Axon Regeneration and Sprouting in Nogo-, MAG-, and OMgp-Deficient Mice. Neuron, 66, 663–670.

Lewerenz J, Klein M, Methner A. (2006). Cooperative action of glutamate transporters and cystine/glutamate antiporter system Xc- protects from oxidative glutamate toxicity. Journal Neurochemistry., 98, 916–925.

Livak and Schmittgen. (2001). Analysis of relative gene expression data using real-time quantitative PCR and the 2(-Delta Delta C(T)). Methods, 25(4), 402-408.

Lopez PHH. (2014). Role of myelin-associated glycoprotein (siglec-4a) in the nervous system. Advanced Neurobiology., 9, 245–262.

Lopez PHH, Ahmad AS, Mehta NR, Toner M, Rowland EA, Zhang J, *et al.* (2011). Myelin-

associated glycoprotein protects neurons from excitotoxicity: Myelin-associated glycoprotein protects neurons. Journal Neurochemistry., 116, 900–908.

Macrez R, Stys PK, Vivien D, Lipton SA, Docagne F. (2016). Mechanisms of glutamate toxicity in multiple sclerosis: biomarker and therapeutic opportunities. Lancet Neurology, 15, 1089–1102.

Marta CB, Taylor CM, Cheng S, Quarles RH, Bansal R, Pfeiffer SE. (2004). Myelin associated glycoprotein cross-linking triggers its partitioning into lipid rafts, specific signaling events and cytoskeletal rearrangements in oligodendrocytes. Neuron Glia Biology, 1(1), 35-46.

Mavrantoni A, Thallmair V, Leitner MG, Schreiber DN, Oliver D, Halaszovich CR. (2015). A method to control phosphoinositides and to analyze PTEN function in living cells using voltage sensitive phosphatases. Frontiers in Pharmacology, 6, 68. doi. 10.3389/fphar.2015.00068.

McKerracher L, Rosen KM. (2015) MAG, myelin and overcoming growth inhibition in the CNS. Frontiers Molecular Neuroscience, 8, 51.

Mecha M. (2011). An easy and fast way to obtain a high number of glial cells from rat cerebral tissue: A beginners approach. Protocol Exchange. doi:10.1038/protex.2011.218. Available from: http://www.nature.com/protocolexchange/protocols/2051.

Meyer-Franke A., Tropak M.B., Roder J.C., Fischer P., Beyreuther K., Probstmeier R., and Schachner M. (1995). Functional Topography of Myelin- Associated Glycoprotein. II. Mapping of Domains on Molecular Fragments. Journal of Neuroscience Research 41:311-323.

Morales-Pantoja IE, Hu C, Perrone-Bizzozero NI, Zheng J, Bizzozero OA. (2016). Nrf2-dysregulation correlates with reduced synthesis and low glutathione levels in experimental autoimmune encephalomyelitis. Journal Neurochemistry,139(4), 640-650

Morrison BM, Lee Y, Rothstein JD. (2013) Oligodendroglia: metabolic supporters of axons. Trends in Cell Biology., 23, 644–651.

Myllykoski M, Eichel MA, Jung RB, Kelm S, Werner HB, Kursula P. High-affinity heterotetramer formation between the large myelin-associated glycoprotein and the dynein light chain DYNLL1. J

Neurochem. 2018; 147(6):764-783.

Nedergaard M, Takano T, Hansen AJ. (2002). Beyond the role of glutamate as a neurotransmitter. Nature Review in Neurosciences, 3, 748–755.

Nelissen K, Smeets K, Mulder M, Hendriks JJA, Ameloot M. (2010). Selection of reference genes for gene expression studies in rat oligodendrocytes using quantitative real time PCR. Journal Neurosciences Methods, 187, 78–83.

Nguyen T, Mehta NR, Conant K, Kim K-J, Jones M, Calabresi PA, *et al.* (2009). Axonal protective effects of the myelin-associated glycoprotein. Journal Neurosciences, 29, 630–637.

Nishioka T, Aoki K, Hikake K, Yoshizaki H, Kiyokawa E, Matsuda M. (2008). Rapid Turnover Rate of Phosphoinositides at the Front of Migrating MDCK Cells. Molecular Biology of the Cell, 19, 4213–4223.

Offen D, Gilgun-Sherki Y, Melamed E. (2004). The role of oxidative stress in the pathogenesis of multiple sclerosis: The need for effective antioxidant therapy. Journal of Neurology, 251, 261–268.

Oka A, Belliveau MJ, Rosenberg PA, Volpe JJ. (1993). Vulnerability of oligodendroglia to glutamate: pharmacology, mechanisms, and prevention. Journal Neuroscience, 13, 1441–1453.

Okumoto S, Looger LL, Micheva KD, Reimer RJ, Smith SJ, Frommer WB. (2005). Detection of glutamate release from neurons by genetically encoded surface-displayed FRET nanosensors. Proceedings of the National Academy of Sciences U. S. A., 102, 8740–8745.

Palandri A, Salvador VR, Wojnacki J, Vivinetto AL, Schnaar RL, Lopez PHH. (2015). Myelin-associated glycoprotein modulates apoptosis of motoneurons during early postnatal development via NgR/p75^{NTR} receptor-mediated activation of RhoA signaling pathways. Cell Death & Disease, 6: e1876.

Pampliega O, Domercq M, Soria FN, Villoslada P, Rodríguez-Antigüedad A, Matute C. (2011). Increased expression of cystine/glutamate antiporter in multiple sclerosis. Journal of Neuroinflammation, 8, 63.

Piani D, Frei K, Do KQ, Cuénod M, Fontana A. (1991). Murine brain macrophages induced NMDA receptor mediated neurotoxicity in vitro by secreting glutamate. Neuroscience Letter., 133, 159–162.

Pitt D, Nagelmeier IE, Wilson HC, Raine CS. (2003) Glutamate uptake by oligodendrocytes: Implications for excitotoxicity in multiple sclerosis. Neurology, 61, 1113–1120.

Pitt D, Werner P, Raine CS. (2000a). Glutamate excitotoxicity in a model of multiple sclerosis. Nature Medicine, 6, 67–70.

Poltorak M, Sadoul R, Keilhauer G, Landa C, Fahrig T, Schachner M. (1987). Myelin-associated glycoprotein, a member of the L2/HNK-1 family of neural cell adhesion molecules, is involved in neuron-oligodendrocyte and oligodendrocyte-oligodendrocyte interaction. Journal of Cell Biology, 105, 1893–1899.

Pronker MF, Lemstra S, Snijder J, Heck AJ, Thies-Weesie DM, Pasterkamp RJ, Janssen BJ.(2016). Structural basis of myelin-associated glycoprotein adhesion and signalling. Nat Commun. 2016; 7:13584.

Quarles RH. (2007). Myelin-associated glycoprotein (MAG): past, present and beyond. Journal Neurochemistry, 100, 1431–1448.

Rosin C, Bates TE, Skaper SD. (2004). Excitatory amino acid induced oligodendrocyte cell death in vitro: receptor-dependent and -independent mechanisms. Journal Neurochemistry, 90, 1173–1185.

Salzer JL, Holmes WP, Colman DR (1987). The amino acid sequences of the myelin-associated glycoproteins: homology to the immunoglobulin gene superfamily. J Cell Biol;104(4):957-65.

Schmued LC, Stowers CC, Scallet AC, Xu L. (2005). Fluoro-Jade C results in ultra-high resolution and contrast labeling of degenerating neurons. Brain Research, 1035, 24–31.

Simons M, Nave K-A. (2016). Oligodendrocytes: Myelination and Axonal Support. Cold Spring Harbor Perspective Biology, 8: a020479.

Smith T, Groom A, Zhu B, Turski L. (2000). Autoimmune encephalomyelitis ameliorated by AMPA antagonists. Nat Med. ;6(1):62-6.

Srinivasan R, Sailasuta N, Hurd R, Nelson S, Pelletier D. (2005). Evidence of elevated glutamate in multiple sclerosis using magnetic resonance spectroscopy at 3 T. Brain Journal of Neurology, 128, 1016–1025.

Stover JF, Pleines UE, Morganti-Kossmann MC, Kossmann T, Lowitzsch K, Kempski OS. (1997). Neurotransmitters in cerebrospinal fluid reflect pathological activity. European Journal of Clinical Investigation, 27, 1038–1043.

Stys PK, Zamponi GW, van Minnen J, Geurts JJG. (2012). Will the real multiple sclerosis please stand up? Nature Review in Neurosciences, 13, 507–514.

Takahashi JL, Giuliani F, Power C, Imai Y, Yong VW. (2003). Interleukin-1β promotes oligodendrocyte death through glutamate excitotoxicity. Annals Neurology, 53, 588–595.

Thompson HJ, Marklund N, LeBold DG, Morales DM, Keck CA, Vinson M, *et al.* (2006). Tissue sparing and functional recovery following experimental traumatic brain injury is provided by treatment with an anti-myelin-associated glycoprotein antibody. European Journal Neuroscience., 24, 3063–3072.

Tropak MB, Johnson PW, Dunn RJ, Roder JC (1988). Differential splicing of MAG transcripts during CNS and PNS development. Brain Res;464(2):143-55.

Umemori H, Sato S, Yagi T, Aizawa S, Yamamoto T (1994). Initial events of myelination involve Fyn
tyrosine kinase signaling. Nature;367(6463):572-6.

Werner P, Pitt D, Raine CS. (2001). Multiple sclerosis: altered glutamate homeostasis in lesions correlates with oligodendrocyte and axonal damage. Annals Neurology, 50, 169–180.

Wosik K, Ruffini F, Almazan G, Olivier A, Nalbantoglu J, Antel JP. (2004). Resistance of

human adult oligodendrocytes to AMPA/kainate receptor-mediated glutamate injury. Brain Journal of Neurology, 127, 2636–2648.

Yim SH, Toda K, Goda S, Quarles RH (1995). Comparison of the phosphorylation of myelin-associated glycoprotein in cultured oligodendrocytes and Schwann cells. J Mol Neurosci;6(1):63-74.

Figure legends

Figure 1: Antibody-mediated activation of MAG in OLs induces an increase in intracellular glutathione concentration and reduces mitochondrial oxidative stress and prevents mitochondrial potential hyperpolarization induced by Glu.

1a. Rat primary OL cultures were treated with anti-MAG mAb (clone 513) or control mAb (clone 9E10) for 24 h and then exposed to 2 mM glutamate Glu for additional 24 h. The intracellular level of GSH was then quantified using mBCl by confocal microscopy. Treatment for 24 h with 2 mM Glu reduces basal GSH levels (*DGC $p<0.05$). Anti-MAG treatment substantially increases GSH (#DGC $p<0.05$; n= 404 cells) and is able to prevent GSH depletion when exposed to Glu overload. Graph represents average data from three independent experiments. **1b.** Representative images of GSH levels in OLs treated with control mAb or anti-MAG mAb. Upper panel: mBCl fluorescence (blue channel) and mature OL marker CC1 (red channel). Lower panel: mBCl fluorescence intensity in a pseudocolor thermal map (warm colors=high GSH, cold colors= low GSH). **1c.** Time course study on GSH changes in OLs after anti-MAG administration. * GSH reaches a ≈40% increase after 10 h of treatment (n= 434 cells). **1d.** Primary OL cultures were transfected with a vector containing a H_2O_2 biosensor (mitoHyper) to monitor its mitochondrial concentration. Cultures were then treated with anti-MAG mAb or control mAb for 24 h. Anti-MAG treatment reduces basal mitochondrial H_2O_2 by a ≈30%, *$p<0.05$. Graph represents average data from three independent experiments (n=30 cells). **1e.** Representative pseudo-color thermal map of H_2O_2 concentrations (HyPer ratio) in OLs estimated by ratiometric measurement of the excitation/emission pairs 405/515 and 488/515. Cold colors indicate low H_2O_2 levels and warm colors represent high H_2O_2 levels. **1f.** Primary OL cultures were treated with anti-MAG mAb and/or 2 mM Glu as described in 1a for 24 h and then stained with tetramethylrhodamine (TMRE), a live mitochondrial potential dye, and further imaged using a spinning disc microscope. Exposure to Glu resulted in increased fluorescence intensity (increased mitochondrial potential) suggesting early stages of cell death (Kumari *et al.*, 2012), while anti-MAG treatment prior to Glu exposure prevented mitochondrial potential hyperpolarization, displaying fluorescence intensities below control cultures. ($H=58.52$, *$p\leq0.05$, n=553 cells). **1g.** Representative images from OL cultures treated with TMRE described above.

Figure 2: Antibody-mediated activation of MAG promotes extracellular Glu uptake in OLs.

2a. The System xc- pharmacological inhibitor aminoadipic acid (AAA) and PDC, an inhibitor of EAATs prevent GSH increases triggered by MAG activation. Graph represents average data from

three independent experiments (*DGC p < 0.05, n= 1023). **2b.** Antibody-mediated activation of MAG in OLs modulates extracellular Glu concentrations. Rat primary OL cultures were transfected with a pDisplay vector containing a FRET-based glutamate biosensor (FLIPE 1m) to monitor its extracellular levels. Cultures were then treated with anti-MAG mAb or control mAb for 24 h and then exposed to 2 mM Glu for 1 h. Glu challenge produces a decrease on FRET ratio, while 24 h pretreatment with anti-MAG mAb raises FRET ratio to normal levels, indicating decreased Glu concentration on the surrounding OLs microenvironment. Symbols indicate statistical comparison with control untreated cultures (*DGC p <0.05, n= 116 cells). Graph represents average data from three independent experiments. **2c.** Images represent the pseudo-color thermal map of FRET activity from data shown in 2b. Cold colors indicated low FRET activity (high extracellular Glu) and warm colors represent high FRET activity (low extracellular Glu). **2d.** Antibody-mediated activation of MAG in OLs increases Glu uptake via EAAT transporters. Rat primary OL cultures were transfected with a pcDNA3.1 vector containing a FRET-based Glu biosensor (FLIPE 10u) to monitor its intracellular levels. Cultures were then treated with anti-MAG mAb or control mAb for 24 h and then exposed to 2 mM Glu for 30 min. Antibody-mediated MAG crosslinking/activation increases intracellular Glu concentration 30 min after Glu challenge. MAG-driven Glu internalization is hampered in PDC (EAAT inhibitor) treated OL cultures. Graph represents average data from three independent experiments (* DGC p < 0.05, n= 256 cells). **2e.** Pseudocolor thermal maps from confocal images of primary OLs transfected with Flipe 10u biosensor (warm colors: high FRET, low glutamate; cold colors: Low FRET, high glutamate). **2f-g.** Quantification of extracellular Glu concentration by fluorimetry in OL cultures treated with anti-MAG mAb or control mAb for 24 h and then exposed to 2 mM Glu for 1 h (f) or 24 h (g). Anti-MAG mAb reduces extracellular Glu concentration in OLs treated for 24 h to values similar to IgG-treated control cultures (*, p<0.0001).

Figure 3: Antibody-mediated activation of MAG in OLs induces a PKC-dependent activation of Nrf2 and associated antioxidant response elements.

3a. Rat primary OL cultures were treated with anti-MAG mAb or control mAb and then immunostained with a polyclonal Ab against the PKC-dependent activation/phosphorylation site of Nrf2 at serine-40 (Nrf2-serine-40). Anti-MAG treatment for 10 h increases nuclear translocation of Nrf2 (*DGC p<0.05; n=528 cells). **3b.** Confocal Images from OL cultures treated for 10 h with anti-MAG mAb (green) and immunostained with Nrf2-serine-40 Ab (red). OLs nuclei were identified by DAPI staining (blue). **3c.** Western Blot of primary OLs culture homogenates depicting increased Nrf2-serine-40 expression (arrowhead indicates Nrf2-serine-40

isoforms, 66 kDa and ~95–110 kDa band size according to Lua *et al.*, 2013). For quantification purposes, bands for Nrf2-serine-40 isoforms were normalized against α-tubulin and expressed as ratio of Nrf2-serine-40/α-tubulin. **3d.** Calphostin, a specific PKC inhibitor, prevents GSH increase on OLs after MAG activation. Calphostin was added 1 h before anti-MAG treatment of primary OLs. Intracellular levels of GSH were quantified after 24 h using mBCl by confocal microscopy (* DGC $p < 0.05$; n=1981 cells). **3e.** Antibody-mediated activation of MAG increases the mRNA expression of genes containing the ARE sequence associated with an antioxidant response including those related with GSH biosynthesis. Quantification by rtPCR of mRNAs expression for Nrf2, GSR, Gclc and Gclm in OLs treated with anti-MAG mAb for 24 h. Data were normalized against the expression of the housekeeper Rpl13a and expressed as a fold change respect to control mAb-treated cultures (dotted line). Symbols indicate statistical comparison with control cultures (*, $p<0.05$; n=8 cultures). **3f.** Antibody-mediated activation of MAG in OLs induces an increase in the expression of the antiporter system xc-. Rat primary OL cultures were treated with anti-MAG mAb or control mAb for 24 h. The plasma membrane expression of the regulatory chain of system xc- (xCT) was quantified by immunofluorescence using confocal microscopy. (*, $p<0.05$; n= 180 cells)(see Supplementary Figure 1 for representative photomicrographs). **3g.** Antibody-mediated activation of MAG in OLs does not increase the mRNA expression of Glu transporters. Quantification by rtPCR of mRNAs expression for GLAST (EAAT1), GLT1 (EAAT2) and EAAC1 (EAAT3) genes in OLs treated with anti-MAG mAb for 24 h. Data are expressed as a fold change respect to control mAb-treated cultures and normalized against the expression of the housekeeper Rpl13a (dotted line, n=8 cultures). All graphs represent average data from three independent experiments.

Figure 4: Early signaling events of MAG activation via phosphoinositides.

4a. Antibody-mediated activation of MAG in OLs induces a transient increase in phosphatidylinositol 4,5-bisphosphate (PIP2) concentrations. Rat primary OL cultures were transfected with a vector containing a FRET-based PIP_2 biosensor (Frubby) to monitor its membrane levels. Cultures were then treated with anti-MAG mAb and fixed at different times. MAG activation led to a transient increase in PIP_2 (peak at 15 min and then returning to basal levels). Symbols indicate statistical comparison with control (untreated) cultures (*, $p< 0.05$; n=195 cells). Images represent the pseudo-color thermal map of FRET activity. Cold colors indicate low fret activity (low membrane PIP_2) and warm colors represent high FRET activity (high membrane PIP2). **4b.** Antibody-mediated activation of MAG in OLs induces an increase in diacylglycerol (DAG) concentrations. OLs were transfected with a vector containing a FRET-

based DAG biosensor (Digda) to monitor its membrane levels. Cultures were then treated with anti-MAG mAb and analyzed at different time points. Results are in accordance with those from PIP2 analysis, showing an increase of DAG over time after antibody treatment (*p <0.05 at 40 and 60 min from treatment; n=118 cells). Images represent the pseudo-color thermal map of FRET activity. Cold colors indicate low fret activity (low membrane DAG) and warm colors represent high FRET activity (high membrane DAG). All graphs represent average data from three independent experiments.

Figure 5: MAG activation protects neurons from Glu-mediated toxicity in organotypic cultures.

Anti-MAG mAb (2 µg/ml) was administered 24 h before 2 mM Glu treatment of 4 div organotypic cerebellar slice cultures. Cultures were fixed 24 h after Glu treatment and immunostained with NeuN (granular neuron marker) and cleaved caspase 3 (early apoptotic marker). Cultured slices were sampled with confocal microphotographs taken every 5 µm. Granule neurons undergoing apoptosis were identified based on morphology (positive for DNA condensation and blebbing) and inmunocitochemistry (positive for cleaved caspase-3). Apoptotic neurons were counted in samples of 0.02 mm^2. Treatment with 2 mM Glu increases apoptotic granule neurons death (*DGC $p<0.05$; n=22 slices). Anti-MAG treatment for 24 h blocked Glu toxicity on neurons. Photomicrographs of confocal sections from cerebellar organotypic cultures. Arrowheads show granule cells positive por apoptosis, which depicts marked cleaved caspase-3 staining and typical nuclear fragmentation (blebbing).

Figure 6: Anti-MAG mAb treatments exerts a neuroprotective effect in a mouse model of Glu-mediated toxicity.

Adult C57Bl/6 mice received an intrastriatal injection consisting in a single dose of 0.5µl injection of 1M Glu to induce an excitotoxic lesion. At 24 h mice were fixed and brains removed, cryostat sectioned (40 µm) and neurodegeneration detected by Fluoro Jade C staining. Lesion volumes (Fluoro Jade C positive damaged brain areas) were quantified with Fiji software using the volume calculator plug-in Volumest. Anti-MAG mAb treatment 1 h before (**6a**) or after (**6b**) intracranial injection of Glu was effective in reducing tissue damage (decreased lesion volumes) with respect to control mAb (*$p<0.05$; n=16 animals per experiment). Representative slices of control mAb and anti-MAG-treated brains showing Fluoro Jade C staining (light green) are shown.

Figure 7: Anti-MAG mAb treatment diminishes clinical symptoms and reduces axonal

damage in a MOG-induced EAE murine model.

Young adult C57Bl/6 mice were immunized with the peptide 35-50 corresponding to the Myelin Oligodendrocyte Glycoprotein (MOG) to induce a chronic inflammatory demyelination. Mice (n=11) were treated with anti-MAG mAb (n=6) or control mAb (n=5) by intraperitoneal injection of 100µg at days 3, 5 and 6 post immunization. Clinical symptoms were assessed daily for 30 days after immunization, then animals were perfused and axon counts performed at high cervical levels (C3-C5) in the gracile fasciculus. **7a.** Clinical motor assessment in EAE mice (performed as described in Jones *et al.*, 2008). Anti-MAG treatment changes time profiles of disease progression, with later onset and lower clinical scores (*p<0.05). **7b.** Anti-MAG mAb treatment effect on axons from gracile fasciculus of C5 spinal cord sections at 30 days after EAE induction. Induction of EAE triggers an axonal loss of myelinated fibers of ≈50% in mice receiving control mAb respect to naïve (non-EAE mice, n=5) (*p<0.05). In contrast, Anti-MAG-treated mice display reduced axonal loss (n/s difference with non-EAE mice). **7c-e.** Representative micrographs of 1 µm plastic sections stained with toluidine blue at C3-5 cervical region of the spinal cords. **7f-h.** Right panels display higher magnification images of the gracile fasciculus. **7i-j** There is a linear correlation between axon accounts in the gracile fasciculus and mean clinical scores and highest clinical scores.

Supplementary Figure 1: Treatment of OLs with anti-MAG mAb resulted in increased system xCT protein expression. Rat primary OL cultures were treated with anti-MAG mAb or control mAb for 24 h. The plasma membrane expression of the regulatory chain of system xc- (xCT) was quantified by immunofluorescence using confocal microscopy. Figure depicts representative photomicrographs of OLs cultures stained for xCT (green) and MAG (red) protein expression. OLs nuclei were identified by DAPI staining (blue).

Supplementary Figure 2: Pharmacological inhibition of PLC by U-73122 prevents changes on Phosphoinositides driven by MAG activation. Rat primary OL cultures were transfected with vectors containing a FRET based PIP_2 biosensor (Frubby, Figure a, n=87 cells) or a DAG sensor (Digda, Figure b, n=131 cells) to monitor its membrane levels. At the activity peak of PLC (40-60 min) cultures were treated at two different concentrations of U-73122 (5 and 10µM) 1 h before exposed to Anti-MAG mAb for 60 min. Treatment with 10µM U-73122 was found effective to inhibit the changes on PIP_2 (increase at 60 min after Anti-MAG treatment) and DAG (decreasing peak at 40 min post mAb treatment).

Supplementary Figure 3: Expression of MAG in cerebellar organotypic cultures. Organotypic cerebellar slice cultures were grown for 4 days, then fixed for 24 h and immunostained with anti-MAG mAb (clone 513, 2 µg/ml) O.N. and further developed using Alexa 488-conjugated secondary anti-mouse abs to detect MAG expression. A cultured slice was sampled with confocal microphotographs taken every 1 µm, total thickness of 15 µm. Image depicts MAG expression (green) on cell bodies and myelin from OLs. Dapi staining (blue) identified cell nuclei.

Supplementary Table 1: Description of rtPCR primers used in this study.

Declaration of interests

☐The authors declare that they have no known competing financial interests or personal relationships that could have appeared to influence the work reported in this paper.

☒The authors declare the following financial interests/personal relationships which may be considered as potential competing interests:

Pablo H. H. Lopez and Edgardo Cristiano reports financial support was provided by Merck KGaA.

Graphical abstract

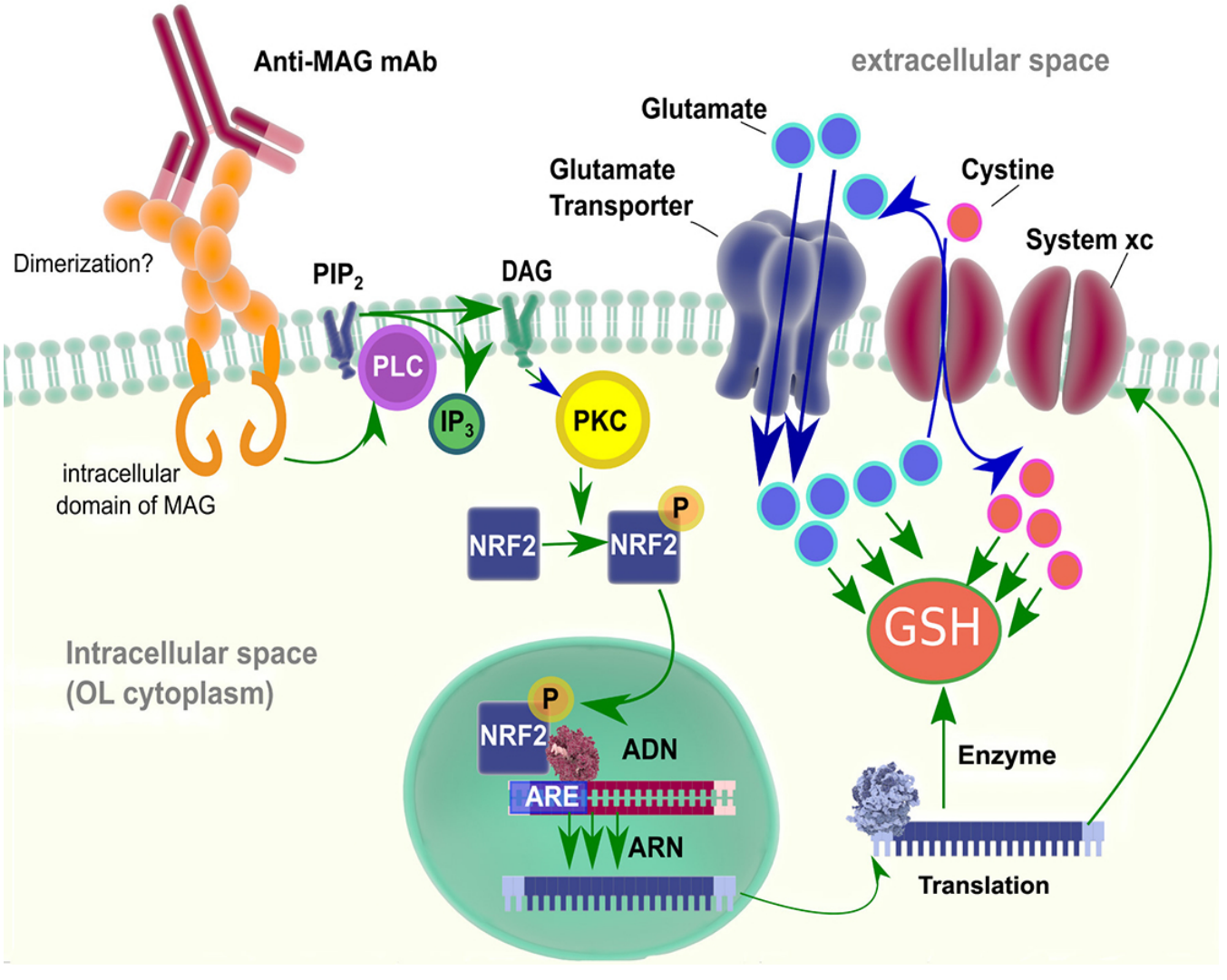

Graphics Abstract

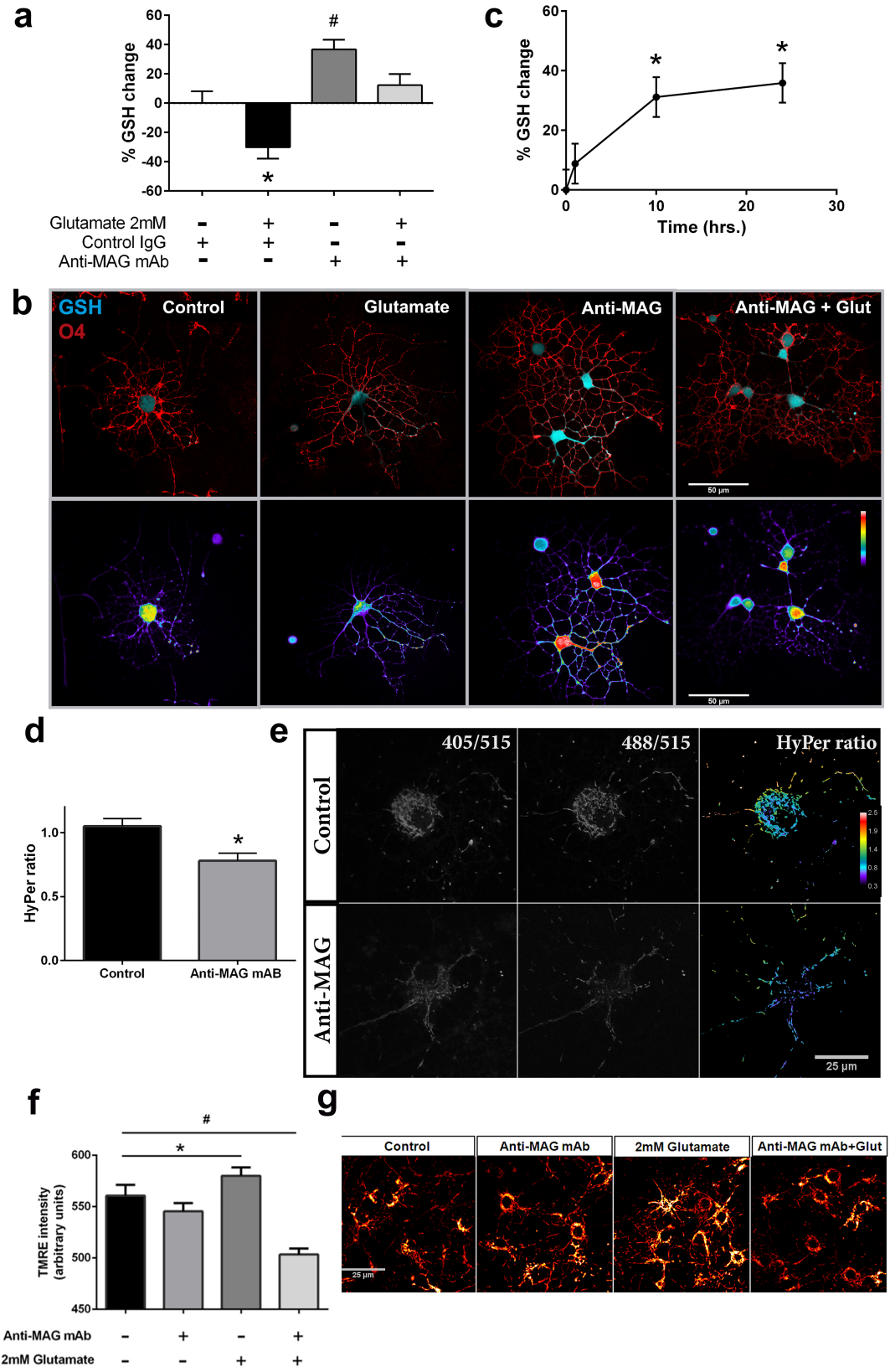
a
% GSH change
60
40
20
0
-20
-40
-60
#
*
Glutamate 2mM - + - +
Control IgG + + - -
Anti-MAG mAb - - + +
c
% GSH change
60
40
20
0
0
10
20
30
Time (hrs.)
*
*
b
GSH
O4
Control
Glutamate
Anti-MAG
Anti-MAG + Glut
50 µm
50 µm
d
HyPer ratio
1.0
0.5
0.0
*
Control
Anti-MAG mAB
e
405/515
488/515
HyPer ratio
Control
Anti-MAG
2.5
1.9
1.4
0.8
0.3
25 µm
f
#
*
TMRE intensity (arbitrary units)
600
550
500
450
Anti-MAG mAb - + - +
2mM Glutamate - - + +
g
Control
Anti-MAG mAb
2mM Glutamate
Anti-MAG mAb+Glut
25 µm

Figure 1

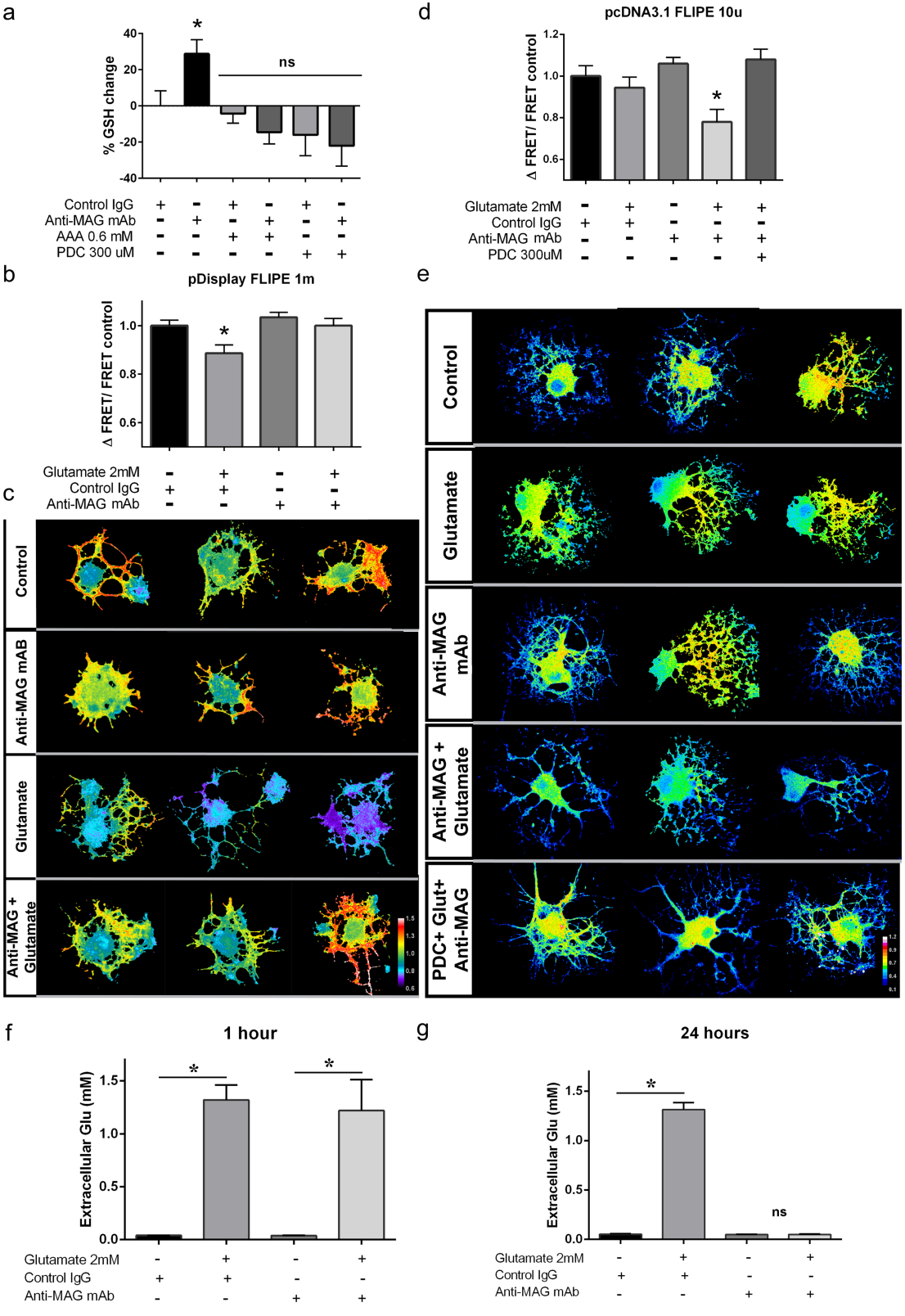
a
% GSH change
40
20
0
-20
-40
*
ns
Control IgG + - + - + -
Anti-MAG mAb - + - + - +
AAA 0.6 mM - - + + - -
PDC 300 uM - - - - + +
d
pcDNA3.1 FLIPE 10u
Δ FRET/ FRET control
1.2
1.0
0.8
0.6
*
Glutamate 2mM - + - + +
Control IgG + + - - -
Anti-MAG mAb - - + + +
PDC 300uM - - - - +
b
pDisplay FLIPE 1m
Δ FRET/ FRET control
1.0
0.8
0.6
*
Glutamate 2mM - + - +
Control IgG + + - -
Anti-MAG mAb - - + +
c
Control
Anti-MAG mAB
Glutamate
Anti-MAG + Glutamate
1.5
1.3
1.0
0.8
0.6
e
Control
Glutamate
Anti-MAG mAb
Anti-MAG + Glutamate
PDC+ Glut+ Anti-MAG
1.2
0.9
0.7
0.4
0.1
f
1 hour
Extracellular Glu (mM)
1.5
1.0
0.5
0.0
*
*
Glutamate 2mM - + - +
Control IgG + + - -
Anti-MAG mAb - - + +
g
24 hours
Extracellular Glu (mM)
1.5
1.0
0.5
0.0
*
ns
Glutamate 2mM - + - +
Control IgG + + - -
Anti-MAG mAb - - + +

Figure 2

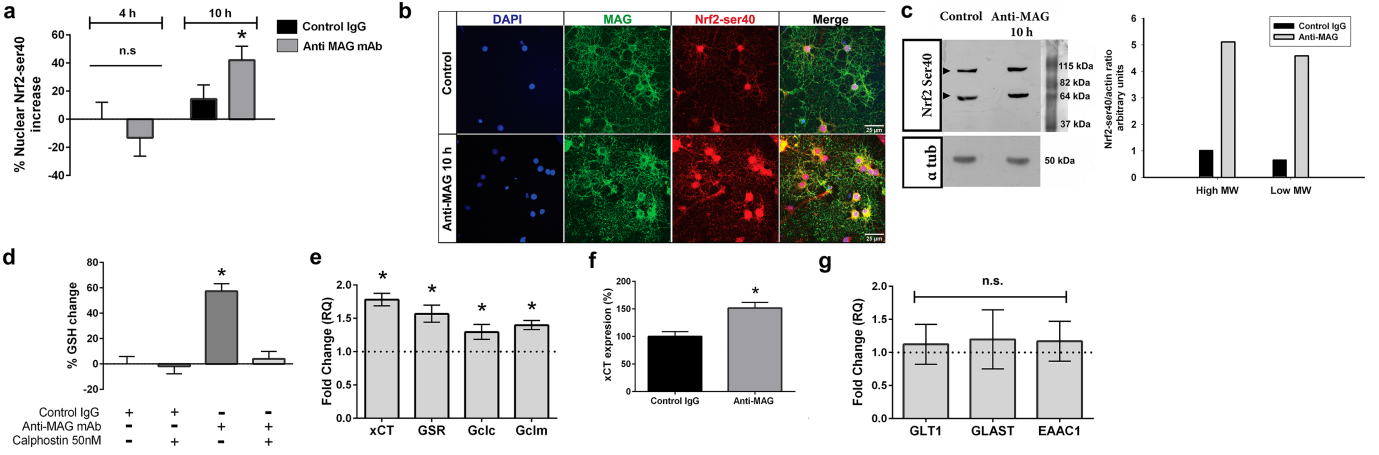
a
4 h
10 h
n.s
*
Control IgG
Anti MAG mAb
% Nuclear Nrf2-ser40 increase
b
DAPI
MAG
Nrf2-ser40
Merge
Control
Anti-MAG 10 h
c
Control
Anti-MAG
10 h
Nrf2 Ser40
α tub
115 kDa
82 kDa
64 kDa
37 kDa
50 kDa
Control IgG
Anti-MAG
Nrf2-ser40/actin ratio arbitrary units
High MW
Low MW
d
% GSH change
Control IgG
Anti-MAG mAb
Calphostin 50nM
e
Fold Change (RQ)
xCT
GSR
Gclc
Gclm
f
xCT expresion (%)
Control IgG
Anti-MAG
g
n.s.
Fold Change (RQ)
GLT1
GLAST
EAAC1

Figure 3

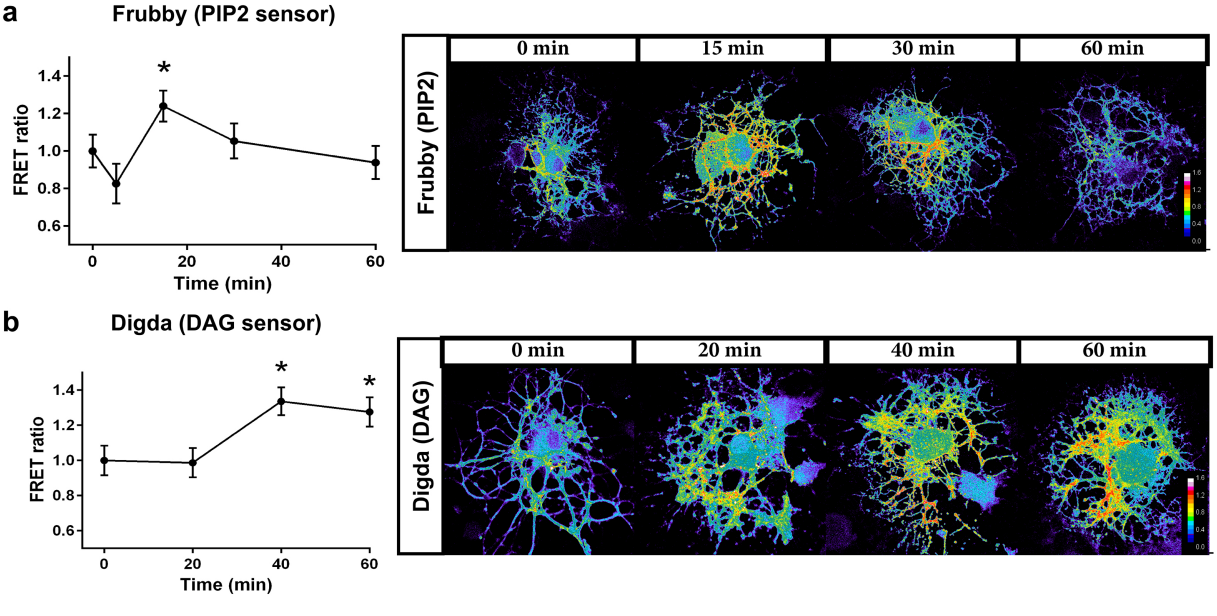
a
Frubby (PIP2 sensor)
FRET ratio
1.4
1.2
1.0
0.8
0.6
*
0
20
40
60
Time (min)
0 min
15 min
30 min
60 min
Frubby (PIP2)
1.6
1.2
0.8
0.4
0.0
b
Digda (DAG sensor)
FRET ratio
1.4
1.2
1.0
0.8
0.6
*
*
0
20
40
60
Time (min)
0 min
20 min
40 min
60 min
Digda (DAG)
1.6
1.2
0.8
0.4
0.0

Figure 4

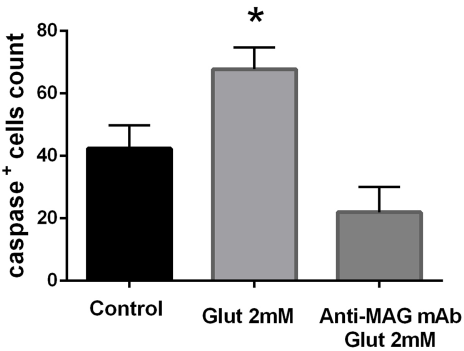
*
caspase+ cells count
80
60
40
20
0
Control
Glut 2mM
Anti-MAG mAb
Glut 2mM

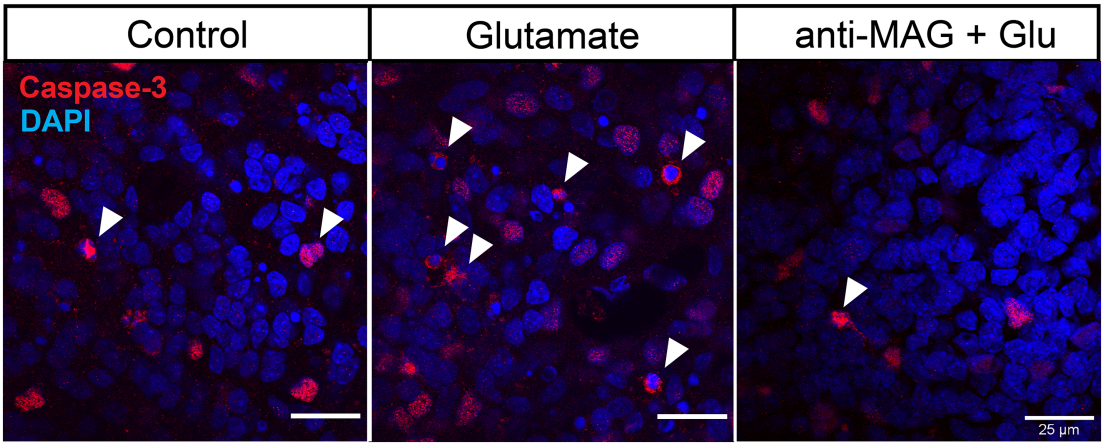
Control
Glutamate
anti-MAG + Glu
Caspase-3
DAPI
25 µm

Figure 5

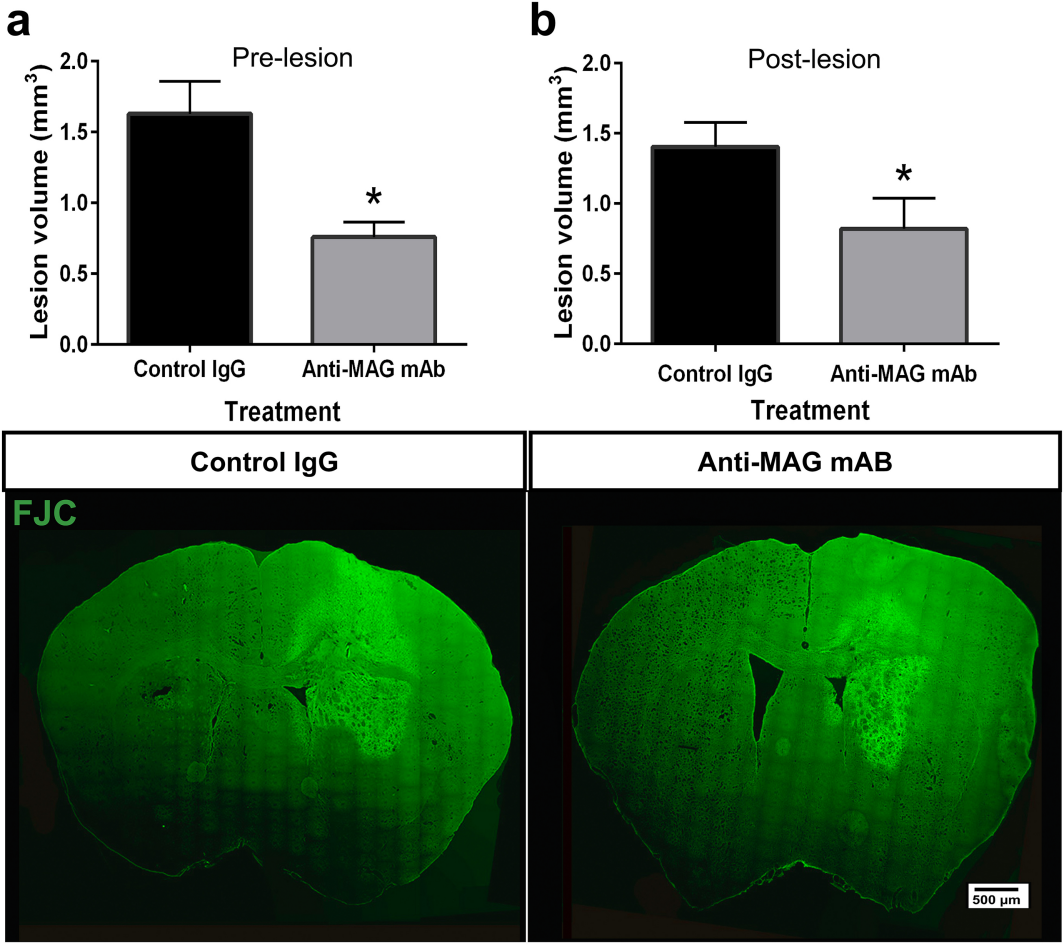
a
Pre-lesion
Lesion volume (mm3)
2.0
1.5
1.0
0.5
0.0
*
Control IgG
Anti-MAG mAb
Treatment
b
Post-lesion
Lesion volume (mm3)
2.0
1.5
1.0
0.5
0.0
*
Control IgG
Anti-MAG mAb
Treatment
Control IgG
Anti-MAG mAB
FJC
500 µm

Figure 6

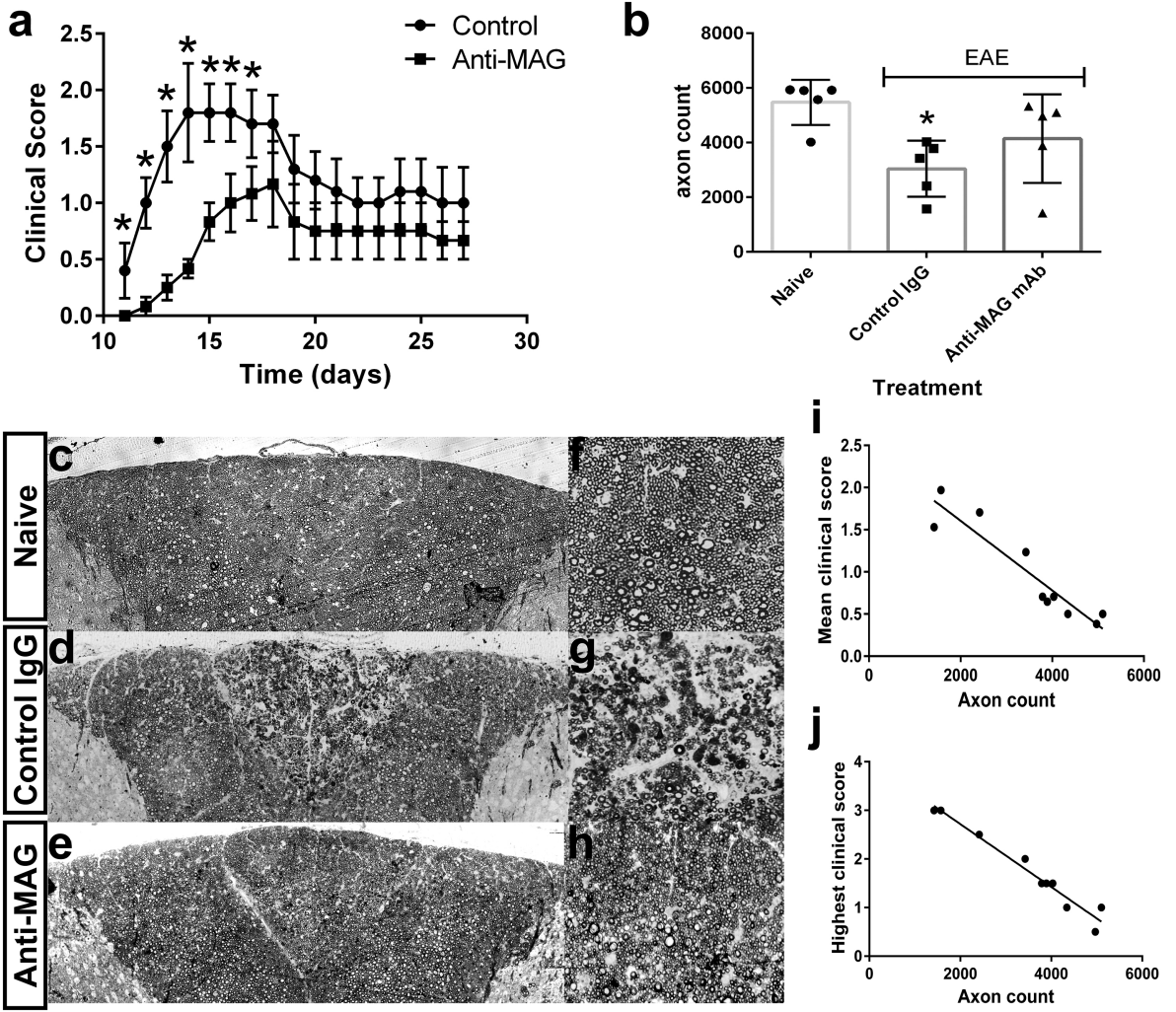
a
Clinical Score
Time (days)
Control
Anti-MAG
b
axon count
EAE
Naive
Control IgG
Anti-MAG mAb
Treatment
c
d
e
f
g
h
Naive
Control IgG
Anti-MAG
i
Mean clinical score
Axon count
j
Highest clinical score
Axon count

Figure 7